ORKUSTOFNUN
NATIONAL ENERGY AUTHORITY

THE UNITED NATIONS UNIVERSITY

RESISTIVITY, INDUCED POLARIZATION, AND SELF-POTENTIAL METHODS IN GEOTHERMAL EXPLORATION

Stanley H. Ward
and
William R. Sill

UNU Geothermal Training Programme, Iceland.
Report 1983-3

RESISTIVITY, INDUCED POLARIZATION, AND SELF-POTENTIAL METHODS IN GEOTHERMAL EXPLORATION

by

Stanley H. Ward
and
William R. Sill

Earth Science Laboratory
University of Utah Research Institute

and

Department of Geology and Geophysics
University of Utah

TABLE OF CONTENTS

II

Page

ABSTRACT

The article commences with an overview of the literature. This is followed by a statement of some elementary electromagnetic theory necessary to establish the MKS system of units and the fundamental physics governing electrical methods of exploration. Next there is presented a reasonably detailed discussion of the electrical properties of earth materials including normal mode of conduction, surface conduction, electrode polarization, membrane polarization, semiconduction, melt conduction, real and complex resistivity, and the origin of self-potentials in geothermal systems.

Electrical resistivity surveys are used routinely and successfully in geothermal exploration. They map regions of thermal brines and/or wall rock alteration resulting from interaction of the thermal brines with the reservoir rocks. The depth of exploration of the dipole-dipole array seldom exceeds 2a, where a is a dipole length, and it is often less than this in areas with conductive overburden. The dipole-dipole method is well-suited to combined sounding and profiling in which application it provides modest lateral and vertical resolution. For improved vertical resolution in sounding the Schlumberger array is best, but it is not convenient for detailed profiling. Other arrays have been used but are not preferred by most practioners. The dipole-dipole array is the only one recommended by us for induced polarization surveys.

Problems encountered in resistivity and induced polarization surveys involve such noise sources as natural fields, cultural fields, overburden, topography, extraneous geological features, and electromagnetic coupling. Each of these noise sources is discussed in relation to the ability of the referenced methods to detect anomalies associated with geothermal systems. A

brief section on modern instrumentation for resistivity and induced polarization surveys follows. An account is then given of applications of induced polarization in geothermal surveys.

Self-potential surveys also are used routinely and successfully in geothermal exploration but quantitative interpretation of the resulting data has only recently emerged. Noise sources in self-potential surveys include telluric currents, electrode drift, topography, variations in soil moisture, culture, vegetation, and moving surface and subsurface non-thermal waters.

To illustrate how members of the Earth Science Laboratory of the University of Utah Research Institute use electrical methods within the framework of integrated geological, geochemical, and geophysical exploration, the case history of the Monroe-Red Hill hot springs system is presented. Both resistivity and self-potential methods have proven successful at this low-temperature, fault-controlled, normal geothermal gradient prospect.

1.0 INTRODUCTION

Electrical resistivity surveys are used routinely in geothermal exploration on a prospect scale. They are of particular importance in mapping faults, fractures, contacts, thermal brines, and zones of hydrothermal alteration. Thermal waters become increasingly conductive with increasing salinity and with increasing temperature up to 300°C above which conductivity decreases. The long-term interaction between thermal fluids and the subsurface environment gives rise to extensive wall rock alteration (Moskowitz and Norton, 1977). The alteration produces conductive mineral assemblages such as clays and may develop additional porosity. This environment of low-resistivity pore fluids and conductive mineral assemblages is a good target for electrical exploration techniques. Hence, exploratory wells are often located with the aid of resistivity surveys. Several different resistivity arrays have been used for this purpose, including the Wenner, Schlumberger, dipole-dipole, and bipole-dipole arrays.

The use of the induced polarization method in geothermal exploration is minimal, for reasons to be discussed. However, we include it here because it holds promise for mapping regions of hydrothermal alteration in geothermal systems. Alteration products such as clay minerals and pyrite produce induced polarization anomalies.

The purpose of this article is to summarize the principles, problems, and applications of the resistivity and self-potential methods in geothermal exploration and to note the circumstances whereby the induced polarization method might be used. The applications will reference recent literature.

The use of the Schlumberger and Wenner arrays have been referenced in Banwell and MacDonald (1965), Hatherton et al. (1966), MacDonald and Muffler

(1972), Meidav and Furgerson (1972), Zohdy et al. (1973), Arnorsson et al. (1975), Gupta et al. (1975), Stanley et al. (1976), Tripp et al. (1978), Razo et al. (1980), and others. Dipole-dipole arrays were used in surveys reported by Klein and Kauahikaua (1975), Jiracek et al. (1975), McNitt (1975), Garcia (1975), Ward et al. (1978), Patella et al. (1979, 1980), Baudu et al. (1980), Wilt et al. (1980), and others. The bipole-dipole array was first used in geothermal exploration by Risk et al. (1970) and subsequently studied by Bibby and Risk (1973), Keller et al. (1975), Risk (1975a,b), Williams et al. (1975), Beyer et al. (1975), Stanley et al. (1976), Jiracek and Smith (1976), Dey and Morrison (1977), Souto (1978), Hohmann and Jiracek (1979), Frangos and Ward (1980), and others. A generalization of the bipole-dipole array, called the quadripole array has been described by Doicin (1976), Bibby (1977), Harthill (1978), and others. The relative advantages of the various arrays will be described subsequently.

Corwin and Hoover (1979) summarized the application of the self-potential method in geothermal exploration to the date of their writing. According to them, "Self-potential surveys conducted in a variety of geothermal areas show anomalies ranging from about 50 mV to over 2 V in amplitude over distances of about 100 m to 10 km. The polarity and waveform of the observed anomalies vary, with positive, negative, bipolar, and multipolar anomalies having been reported from different areas. Steep potential gradients often are seen over faults which are thought to act as conduits for thermal fluids. In some areas, anomalies several kilometers wide correlate with regions of known elevated thermal gradient or heat flow." Sill (1981, 1982a,b,c) has made significant progress in developing quantitative interpretation methods for application to self-potential surveys.

2.0 BASIC ELECTROMAGNETIC THEORY

2.1 Introduction

We present, now, theory sufficient only for the purposes of this article. Throughout, MKS units will be used and a time dependence $e^{i\omega t}$ will be invoked.

2.2 Maxwell's Equations

An electromagnetic field may be defined as the domain of the four vector functions, $\vec{E}$, $\vec{B}$, $\vec{D}$, $\vec{H}$ where:

$\vec{E}$ is the electric field intensity in volt/m,

$\vec{B}$ is the magnetic induction in weber/m^2,

$\vec{D}$ is the dielectric displacement in coulomb/m^2

and

$\vec{H}$ is the magnetic field intensity in ampere-turn/m.

The experimental evidence of Ampere and Faraday leads to the two fundamental Maxwell equations described in the time domain:

$$\nabla \times \vec{E} + \frac{\partial \vec{B}}{\partial t} = 0, \tag{1}$$

and

$$\nabla \times \vec{H} - \frac{\partial \vec{D}}{\partial t} = \vec{J}, \tag{2}$$

in which $\vec{J}$ is the electric current density and $\frac{\partial \vec{D}}{\partial t}$ is the displacement current density, both in amp/m^2. If one takes the divergence of (1) and (2), he obtains

$$\nabla \cdot \frac{\partial \vec{B}}{\partial t} = 0,$$

and (3)

$$-\nabla \cdot \frac{\partial \vec{D}}{\partial t} = \nabla \cdot \vec{J}.$$

because the divergence of a curl is zero. Provided the vector functions $\vec{B}$ and $\vec{D}$ are piecewise continuous and possess continuous first and second derivatives, then the operators $\nabla \cdot$ and $\frac{\partial}{\partial t}$ may be interchanged to yield

$$\frac{\partial}{\partial t} (\nabla \cdot \vec{B}) = 0, \tag{4}$$

and

$$- \frac{\partial}{\partial t} (\nabla \cdot \vec{D}) = \nabla \cdot \vec{J}. \tag{5}$$

Equation (4) yields the third Maxwell equation

$$\nabla \cdot \vec{B} = 0 \tag{6}$$

if at any time $\vec{B}$ was zero. Equation (5) yields the fourth Maxwell equation

$$\nabla \cdot \vec{D} = \rho_e \tag{7}$$

if at any time $\vec{D}$ was zero, provided that an equation of continuity

$$\nabla \cdot \vec{J} + \frac{\partial \rho_e}{\partial t} = 0 \tag{8}$$

is applied. Equation (8) is a statement of the conservation of charge in the vicinity of a point (Stratton, 1941, p. 5). For *homogeneous* earth materials of conductivity 10^{-4} mhos/m or greater, free charge ρ_e dissipates in less than 10^{-6} seconds (Stratton, 1941, p. 15). Thus for geophysical prospecting, in which frequencies less than 10^5 Hz are employed, $\frac{\partial \rho_e}{\partial t} \sim 0$, and we may write

$$\nabla \cdot \vec{J} = 0. \tag{9}$$

Equation (9) does not apply to inhomogeneous regions; at the interface between two different media a surface charge accumulates.

2.3 The Constitutive Relations

The first two Maxwell equations, equations (1) and (2), are uncoupled differential equations describing the experimental behavior of the five vector functions, $\vec{E}$, $\vec{B}$, $\vec{H}$, $\vec{D}$, and $\vec{J}$. These two equations are only coupled through the frequency domain constitutive relations

$$\vec{D} = \tilde{\tilde{\varepsilon}}\,(\omega, \vec{E}, \vec{r}, t, T, P, \ldots) \cdot \vec{E}\,, \tag{10}$$

$$\vec{B} = \tilde{\tilde{\mu}}\,(\omega, \vec{B}, \vec{r}, t, T, P, \ldots) \cdot \vec{H}\,, \tag{11}$$

and

$$\vec{J} = \tilde{\tilde{\sigma}}\,(\omega, \vec{E}, \vec{r}, t, T, P, \ldots) \cdot \vec{E}\,, \tag{12}$$

in which the tensors, $\tilde{\tilde{\varepsilon}}$, $\tilde{\tilde{\mu}}$, $\tilde{\tilde{\sigma}}$ describe, respectively, the dielectric permittivity, the magnetic permeability, and the electric conductivity as functions of angular frequency ω, electric field strength $\vec{E}$ or magnetic induction $\vec{B}$, position $\vec{r}$, time t, temperature T, and pressure P. Each of these three tensors is complex in the general case, permitting the phases of $\vec{D}$ and $\vec{E}$, of $\vec{H}$ and $\vec{B}$, and of $\vec{J}$ and $\vec{E}$ to be different. In most elementary electromagnetic earth problems the following assumptions are made in order to simplify analysis.

1) All media are linear, isotropic, homogeneous, and possess electrical properties which are independent of time, temperature, or pressure.

2) The magnetic permeability μ is assumed to be that of free space, i.e., $\mu = \mu_0$.

These assumptions are made in some applications. Exceptions follow:

1) Anisotropic media are included in some simple electromagnetic boundary value problems and aid in interpretation of data obtained with plane wave sources.

2) Inhomogeneous media entering into electromagnetic boundary value problems are treated as one-dimensionally inhomogeneous (plane-layered), two-dimensionally inhomogeneous (infinite cylinders of arbitrary cross-section) or three-dimensionally inhomogeneous.

3) In geothermal exploration, attempts have been made to determine temperature from electrical conductivity measurements, but these have not generally been successful because conductivity is much more affected by pore water salinity, for example, than by temperature.

4) In shallow prospecting the effect of pressure is small and is customarily ignored.

5) The time dependence of electrical conductivity due to varying moisture content in surface soils is usually ignored although not correctly so.

For the purpose of subsequent discussion, the following three constitutive relations will suffice:

$$\vec{D} = [\varepsilon'(\omega) - i\varepsilon''(\omega)]\vec{E} = \varepsilon\vec{E}, \tag{13}$$

$$\vec{J} = [\sigma'(\omega) + i\sigma''(\omega)]\vec{E} = \sigma\vec{E}, \tag{14}$$

and

$$\vec{B} = \mu\vec{H}, \tag{15}$$

in which dielectric permittivity ε and electrical conductivity σ are complex functions of angular frequency while magnetic permeability μ is independent of frequency and is real.

2.4 The Wave Equations

If we replace each of the five field vector functions, $\vec{B}$, $\vec{D}$, $\vec{H}$, $\vec{E}$, and $\vec{J}$, by an expression of the form $\vec{A} = \vec{A}_o e^{i\omega t}$ equations (1) and (2) become, with the aid of the constitutive relations (13), (14) and (15), Maxwell's equations in the frequency domain

$$\nabla \times \vec{E} + i\mu\omega \vec{H} = 0, \tag{16}$$

and

$$\nabla \times H - (\sigma + i\varepsilon\omega) \vec{E} = 0. \tag{17}$$

The factor $\vec{A}_o$ is the complex vector amplitude while the factor $e^{i\omega t}$ is the general harmonic describing sinusoidal behavior of the fields. We may now introduce the impeditivity ($\hat{z} = i\mu\omega$) and the admittivity ($\hat{y} = \sigma + i\varepsilon\omega$) Harrington (1961) so that (16) and (17) are written

$$\nabla \times \vec{E} + \hat{z} \vec{H} = 0, \tag{18}$$

and

$$\nabla \times \vec{H} - \hat{y} \vec{E} = 0. \tag{19}$$

If we now take the curl of (18), we obtain

$$\nabla \times \nabla \times \vec{E} + \hat{z} \nabla \times \vec{H} = 0, \tag{20}$$

and substitution of (19) yields

$$\nabla \times \nabla \times \vec{E} + \hat{z}\hat{y} \vec{E} = 0. \tag{21}$$

The vector identity in cartesian coordinates

$$\nabla \times \nabla \times \vec{A} \equiv \nabla\nabla \cdot \vec{A} - \nabla^2 \vec{A}, \tag{22}$$

where $\vec{A}$ is any vector, and the divergenceless electric field, applicable in *homogeneous* regions,

$$\nabla \cdot \vec{E} = 0, \tag{23}$$

convert (21) to

$$\nabla^2 \vec{E} - \hat{z}\hat{y} \vec{E} = 0, \tag{24}$$

or

$$\nabla^2 \vec{E} + k^2 \vec{E} = 0, \tag{25}$$

where

$$k = \sqrt{- \hat{z}\hat{y}} = \sqrt{\mu\omega(\varepsilon\omega - i\sigma)} \tag{26}$$

is the wave number and it is understood that ε and σ are complex functions of angular frequency ω. Equation (25) is the *homogeneous* wave equation for electric field, in the frequency domain, for homogeneous media. Elementary plane wavelet solutions of the electric field wave equation are of the form

$$\vec{E} = \vec{E}_o \, e^{-i(kz - \omega t)} \, . \tag{27}$$

The wave equation, in the frequency domain, for magnetic field is derived similarly and is

$$\nabla^2 \vec{H} + k^2 \vec{H} = 0, \tag{28}$$

with solutions

$$\vec{H} = \vec{H}_o e^{-i(kz - \omega t)} \, . \tag{29}$$

It can be established readily that (27) and (29) represent waves travelling in the positive z direction whereas a wave with e^{ikz} in the phase term represents a wave travelling in the negative z direction.

2.5 Complex Conductivity, Relative Magnetic Permeability, and Dielectric Constant

The total current density $\nabla \times \vec{H}$ of equation (17) is made up of a part $\sigma\vec{E}$, the conduction current, which is in-phase with the electric field intensity for real σ, and a part $i\varepsilon\omega\vec{E}$, the displacement current, which is in quadrature with the electric field intensity for real ε. When both σ and ε are complex, the association of conduction current with in-phase and displacement current with quadrature is no longer possible. Thus for general earth media we usually write

$$k^2 = -i\mu\omega\,[\sigma'(\omega) + i\sigma''(\omega)], \tag{30}$$

or

$$k^2 = -i\mu\omega|\sigma(\omega)|\,e^{i\phi(\omega)}\,, \tag{31}$$

in which real and imaginary parts of dielectric permittivity have become absorbed into imaginary and real parts, respectively, of electrical conductivity. The form (31) is used for wet earth materials, where $|\sigma(\omega)|$ is the amplitude and $\phi(\omega)$ is the phase of conductivity.

The dielectric constant is defined as the dimensionless quantity

$$K_e = \varepsilon/\varepsilon_0, \tag{32}$$

and the relative magnetic permeability as the dimensionless quantity

$$K_m = \mu/\mu_0\,, \tag{33}$$

where ε_0 has the free space value 8.854×10^{-12} farad/meter while μ_0 has the free space value $4\pi \times 10^{-7}$ henry/meter.

3.0 ELECTRICAL PROPERTIES OF EARTH MATERIALS

3.1 Introduction

Bulk resistivities from the surface to in excess of 15 km depth in a normal crust are controlled by aqueous electrolytic conduction via pores, fractures, and faults. A slight increase in resistivity with depth in this region is the result of decreasing pore, fracture and fault porosity due to increased hydrostatic load. Fractures and faults are known to remain open to depths in excess of 5 km due to departures from hydrostatic loading. From about 15 km to the Moho, mineral semiconduction dominates and the resistivity decreases downwards. Semiconduction will remain the dominant conduction mechanism in excess of 100 km into the normal upper mantle.

In spreading centers (e.g. Iceland), intraplate melting zones (e.g. Hawaiian Islands), hot spots (e.g. Yellowstone, USA), subduction zones (e.g. Cascades volcanoes, USA and Canada), extensional continental regions (e.g. eastern Basin and Range, USA), and rift zones (e.g. East African Rift), the crust and mantle are abnormal in that they then contain melt or partial melt at any depth from surface to 100 km. Thus in geothermal areas, which abound in the tectonically active areas, one must be concerned with three basically different conduction mechanisms: aqueous electrolyte conduction, semiconduction, and melt conduction.

3.2 Aqueous Electrolyte Conduction

3.2.1 Normal mode of conduction

Conduction in near-surface rocks is largely electrolytic, taking place in pore spaces, along grain boundaries, in fractures and in faults but negligibly through the silicate framework.

The ions which conduct the current result from the dissociation of salts, such dissociation occurring when salts are dissolved in water. Since each ion is able to carry only a definite quantity of charge, it follows that the more ions that are available in a solution and the faster they travel, the greater will be the charge that can be carried. Hence, the solution with the larger number of ions will have the higher conductivity. Thus, in general, a rock which contains saline water within its pores will have a greater conductivity when the salinity of the water is high than when it is low; salinity is a major factor in determining the resistivity of a rock.

An increase in temperature lowers the viscosity of water, with the result that ions in the water become more mobile. The increased mobility of the ions results in an observed resistivity decrease with increase in temperature according to the formula

$$\rho_t = \frac{\rho_{18}}{1 + \alpha\,(t - 18)} \tag{34}$$

in which α is the temperature coefficient of resistivity (usually given as about 0.025 per degree centigrade), t is the ambient temperature, ρ_t is the resistivity at this temperature, while ρ_{18} is the resistivity at 18°C.

Archie's Law,

$$F = \frac{\rho_r}{\rho_w} = \phi^{-m}\ , \tag{35}$$

usually is satisfied for aqueous electrolytic conduction. In (35), F is formation factor, ρ_r is the resistivity of the rock, ρ_w is resistivity of the saturating electrolyte, ϕ is porosity, and m is

the cementation factor which usually varies between 1.5 and 3.

3.2.2 The effect of clays on rock resistivity

A clay particle acts as a separate conducting path additional to the electrolyte path. The resistance of this added path is low. The origin of this abnormally high clay mineral conductivity lies in the double layer of exchange cations as shown in Figure 1. The cations are required to balance the charge due to substitution within the crystal lattice, and to broken bonds (Grim, 1953). The finite size of the cations prevents the formation of a single layer. Rather, a *double layer* is formed; it consists of a *fixed layer* immediately adjacent to the clay surface and a *diffuse layer* which drops off in density exponentially with distance from the fixed layer.

The diffuse layer, in contrast to the fixed layer, is free to move under the influence of an applied electric field. The cations of the diffuse layer add to the normal ion concentration and thus increase the density of charge carriers. The net result is an increased *surface conductivity*. Although clay minerals exhibit this property to a high degree because of their large ion exchange capacity, all minerals exhibit it to a minor extent. All rocks containing clay minerals possess an abnormally high conductivity on this account.

The effect of disseminated clay or shale on rock resistivities becomes increasingly important as the conductance through the pores diminishes. In a geothermal environment, hydrothermal alteration converts feldspars to kaolinite,

montmorillonite and other clay minerals, especially in silicic rocks. In basic rocks, chlorite and serpentine may also be produced. All of these alteration products exhibit high surficial conductivity. As the concentration of the electrolyte increases, the relative contribution of the electrolyte conduction path to the clay conduction path increases as may be seen from the formula

$$\sigma_r = \frac{\sigma_e + \sigma_s}{F} \qquad (36)$$

in which σ_r, σ_e, and σ_s represent the observed conductivities of the rock, the electrolyte, and the clay surface path. Ward and Sill (1976) demonstrate that $\sigma_s \sim 3\ \sigma_e$ for altered rocks at Roosevelt Hot Springs, Utah, USA, despite the presence of an electrolyte containing 7000 ppm total dissolved solids.

3.3 Induced Polarization in Geothermal Areas

3.3.1 Introduction

Pyrite and clay minerals often are found as alteration products in geothermal areas. Hence the induced electrical polarization mechanisms of electrode polarization and membrane polarization might be expected in these areas.

3.3.2 Electrode polarization

Whenever there is a change in the mode of current conduction, e.g. from ionic to metallic, energy is required to cause the current to flow across the interface. This energy barrier can be considered to constitute an electrical impedance.

The surfaces of most solids possess a very small net attraction for either cations or anions, as we mentioned earlier for

clay minerals. Immediately adjacent to the outermost solid layer is adsorbed a layer of essentially fixed ions, one or a few molecular layers in thickness (Figure 2a). These are not truly exchangeable and, hence, constitute the fixed layer.

Adjacent to the fixed layer of adsorbed ions there is a group of relatively mobile ions, either of the same or opposite charge, known as the diffuse layer. The *anomalous* number of ions in this zone decreases exponentially from the fixed layer outward to the normal ion concentration of the liquid. (The normal balanced distribution of anions and cations has been deleted from Figure 2 for clarity). The particular distribution of ions shown is only one of several possible distributions, but it is the most common. The electrical potential across the double layer has been plotted also; the potential drop across the diffuse layer is known as the Zeta potential (Z).

While the fixed layer is relatively stable, the diffuse layer thickness is a function of temperature, ion concentration in the *normal* electrolyte, valency of the ions, and the dielectric constant of the medium. Most of the anomalous charge is contained within a plane distance d from the surface, where (Grahame, 1947)

$$d = \left[\frac{\varepsilon_o K_e kT}{2ne^2v^2}\right]^{1/2}, \qquad (37)$$

n = normal ion concentration of the electrolyte,

v = valence of the normal ions,

e = elementary charge,

K_e = the dielectric constant of the medium,

k = Boltzman's constant,

and

T = temperature.

The thickness is, therefore, governed by the balance between the attraction of unlike charges at the solid surface and the thermal redistribution of ions. Obviously, increasing n, the salinity, or v, the valence, decreases the diffuse layer thickness.

Returning now to polarization at electrodes, it may be stated that there are two paths by which current may be carried across an interface between an electrolyte and a metal (Figure 3). These are called the faradaic and nonfaradaic paths. Current passage in the faradaic path is the result of an electrochemical reaction such as the oxidation or reduction of some ion, and may involve the diffusion of the ions toward or away from the interface. The charge is carried physically across the interface by an electron transfer. In the latter, i.e. nonfaradaic, case, charged particles do not cross the interface; rather, current is carried by the charging and discharging of the double layer. The nonfaradaic component, thus, may be represented by a simple capacitance insofar as the variation of its impedance with frequency is concerned.

In the faradaic path, the impedance associated with the electron transfer is represented by the reaction resistance. The ion diffusion process is not representable in so simple a fashion and, in fact, may not be adequately represented by any combination of fixed capacitors and resistors. It is customarily referred to as the Warburg impedance W and its magnitude varies inversely with the

square root of the electrical frequency.

The interfacial impedances of many metal-electrolyte interfaces may be described roughly as follows. Above 1,000 Hz the major part of the electric current is carried across the interface by means of the non-faradaic path; hence, the interfacial impedance varies with frequency as approximately f^{-1}. As the frequency is lowered, more and more current is carried via the faradaic path, and so the low frequency impedance varies with frequency in the range $f^{-1/2}$ to f^{0} depending on the magnitude of the impedance ratio W/R.

All of the above discussion applies to an ideal electrode in a pure electrolyte. The concepts, however, are important in understanding the processes occurring when current is passed through a rock. Any rock sample is *dirty* from the viewpoint of the physical chemist since the electrodes (metallic mineral grains) and electrolytes (pore solutions) are anything but pure. Nevertheless we perhaps are justified in employing equivalent circuits based on pure systems since a phenomenological explanation for rock behavior results. With this caution, one might suggest the equivalence of the elementary rock system of Figure 4a with the equivalent circuit of Figure 4b, where

W is the Warburg impedance

[= $k(1 - i)/ f^{1/2}$; k is a constant],

C_F is the double layer capacitance,

C_{CH} is the chemical capacitance,

R is the reaction resistance,

R' is the resistance representing a higher order reactions,

R_i is the resistance of ionic path,

and

R_m is the resistance of metallic vein path or particle.

In noting these circuit elements, it must be appreciated that one chemical reaction at the interface may lead to a chain of subsequent reactions involving electrons, ions, and molecules of all reaction products present. At each point of the reaction chain, the accumulation of the reaction product represents a capacitance C_{CH} to the electrode. The escape of the product is achieved either by diffusion, represented by a Warburg impedance W, or by a reaction represented by a resistor R. The product of this reaction in turn follows a similar circuit behavior which we have omitted for simplicity, except to lump all such products as R'.

While the circuits of Figure 4b and 4c satisfy the expected physical/chemical processes in mineralized rock, they are too complicated for practical use. Thus, the simple circuit of Figure 5a is used to predict induced polarization, of both electrode and membrane type, in a rock. The frequency and time domain responses of the circuit of Figure 5a are shown in Figures 5b and 5c, respectively. This is the Cole-Cole model of relaxation used by Pelton et al. (1978).

3.3.3 Membrane polarization.

In rocks containing a few percent clays distributed throughout the rock matrix, membrane polarization is of importance. Membrane polarization arises chiefly in porous rocks in

which clay particles (membranes) partially block ionic solution paths [Figure 6a]. The diffuse *cloud* of cations (double layer) in the vicinity of a clay surface is characteristic of clay-electrolyte systems. On application of an electrical potential, positive charge carriers easily pass through the cationic cloud but negative charge carriers accumulate [Figure 6b]; an ion-selective membrane, therefore, exists.

Consequently, a surplus of both cations and anions occurs at one end of the membrane zone, while a deficiency occurs at the other end. This is because the number of positive charges cannot deviate significantly from the number of negative charges at any one point in space due to the large electric fields which would result if they did so deviate. These ion concentration gradients oppose the flow of current. The overall mobility of ions is reduced by this process. This reduction in mobility is most effective for potential variations which are slow (e.g., 0.1 Hz) with respect to the time of diffusion of ions between adjacent membrane zones. For potential variations which are fast (e.g., 1,000 Hz) with respect to the diffusion time, the mobility of ions is not substantially reduced. Hence, the conductivity of a membrane system increases as electrical frequency increases.

3.4 Semiconduction

The *intrinsic* conductivity of a solid at temperature T is computed from the relation

$$\sigma = |e| \left[n_e \mu_e + n_h \mu_h\right] \tag{38}$$

where n_e, n_h are the electron and hole equilibrium concentrations, and μ_e, and μ_h are the mobilities of electrons and holes respectively while e is the elemental charge.

Kinetic theory leads us to expect a temperature dependence of the form $e^{-E/kT}$ for the concentration of electrons in the conduction band of a solid. Assuming a relatively small variation of mobility with temperature, we are then led (Kittel 1953) to predict a conductivity dependence of the form

$$\sigma = \sigma_o e^{-E_g/2kT} \tag{39}$$

in which E_g is the gap energy, σ_o includes the mobility function, and, in this form, is the conductivity as $T \to \infty$. Boltzmann's constant is k. Thermal, electrical, or optical excitation of electrons across the band of forbidden energy renders the solid conducting.

Impurities and imperfections in the material produce extrinsic conductivity. Above some temperature, impurities may be unimportant so that we define the temperature range above extrinsic conductivity as the intrinsic range in which the previous mechanism is operative.

However, below the intrinsic range, certain types of impurities and imperfections markedly alter the electrical properties of a semiconductor. Extrinsic semiconduction arises by thermal excitation of electrons (occupying intermediate energy levels in the forbidden gap produced by impurities in solid solution) into the unoccupied conduction band, or by the excitation of electrons from the occupied valence band into unoccupied impurity levels.

Ionic conduction in a solid occurs as a result of mobile ions moving through the crystal lattice as a result of defects in it. The simplest imperfection is a missing atom or lattice vacancy (Schottky defect). The diffusion of the vacancy through the lattice constitutes transport of charge. The conduction mechanism above 1,100°C is recognized as ionic because, when an iron electrode is used in contact with a magnesium orthosilicate, iron diffuses into the silicate replacing the magnesium.

Table 1 illustrates the temperature ranges important to extrinsic, intrinsic, and ionic conduction.

3.5 Melt Conduction

A silicic magma chamber can be expected to exhibit a resistivity two to three orders of magnitude lower than its solid rock host as the experiments of Lebedev and Khitarov (1964) have demonstrated. Duba and Heard (1980) measured resistivity on buffered olivene while Rai and Manghnani (1978) measured electrical conductivity of basalts to 1550°C; these latter measurements establish that mafic rocks can demonstrate low resistivities also. Resistivities of order 1 Ω m are to be expected in either silicic or basic melts due to ionic conduction.

For partial melts, the melt phase will serve as an interconnection of low resistivity in a residual crystal matrix of resistivity two or more orders greater and will determine the bulk resistivity (Shankland and Waff, 1977). An Archie's Law dependence is hence expected.

4.0 BASIC PRINCIPLES OF RESISTIVITY AND INDUCED POLARIZATION SURVEYS

4.1 Measurements

The resistivity and induced polarization methods involve the measurement of an impedance, with subsequent interpretation in terms of the subsurface electrical properties, and in turn, the subsurface geology. Basically an impedance is the ratio of the response, i.e. output, to the excitation, i.e. input. In the resistivity and induced polarization (IP) methods, the input is a current injected into the ground between two electrodes and the output is a voltage measured between two other electrodes.

In frequency domain impedance measurements, the input current is a sine wave with frequency f and period $T = 1/f$. The output also is a sine wave, as shown in Figure 7; its amplitude (A) and phase (ϕ) depend upon electrical properties of the earth. In general, the output is delayed by $\phi \times T/2\pi$ seconds relative to the transmitted waveform. Often it is convenient to decompose the output wave into in-phase (real) and quadrature (imaginary) components, as shown in Figure 7. If we denote their peak amplitudes as R and I, respectively, then the amplitude and phase of the output waveform are given by

$$A = \sqrt{R^2 + I^2}\ , \tag{40}$$

and

$$\Phi = \arctan\left(\frac{I}{R}\right). \tag{41}$$

Impedance can also be measured in the time domain, in which case the current is periodically turned on and off. As shown in Figure 8, the

output is the voltage measured at various times when the transmitter current is off. Note that the input again is periodic, because measurements must be made for each of several periods and then added together, or stacked, to eliminate noise. Time and frequency domain measurements are directly related through the Fourier transform and, in that sense, are equivalent. However, in practice, each domain has certain advantages and disadvantages.

There are three basic modes of operation for any electrical method: sounding, profiling, and sounding-profiling. In sounding, the transmitter-receiver separation is changed, or the frequency is changed, and the results are interpreted in terms of a layered earth. Because the earth is usually not layered in geothermal prospecting, we believe that sounding has only modest application. In profiling, the transmitter or receiver, or both, are moved along the earth to detect lateral anomalies. The most useful method is a combination of sounding and profiling which delineates both lateral and vertical variations.

Electrical methods have become more useful in recent years through advances in both instrumentation and interpretation. Modern field instruments are based on microcomputers. Processing the signals digitally greatly increases the accuracy and, in fact, makes possible new types of measurements. Further, data reduction in the field facilitates more reliable results and more cost-effective surveys.

The resistivity and induced polarization methods are based on the response of earth materials to the flow of current at low frequencies. The dc resistivity method is based on potential theory which requires direct current, but noise and measurement problems quickly lead to the

use of alternating currents (ac) of low frequency, so that the resistivity method now employs ac exclusively. The induced polarization method, on the other hand, requires the use of alternating current because it is based on changes in resistivity as a function of frequency. As the frequency increases, in some critical frequency range determined by the resistivity of the materials and the scale size of the measurement, electromagnetic coupling between transmitting and receiving circuits violates potential theory so that electromagnetic theory is required.

Measurements are made with a four-electrode array consisting of two current and two potential electrodes. Resistivity data always are recorded along with induced polarization to aid in interpretation. For a homogeneous earth, the resistivity is given by

$$\rho = K \frac{\Delta V}{I} , \qquad (42)$$

where I is the current, ΔV is the measured potential difference, and K is a geometric factor that depends on the electrode configuration. When the ground is not homogeneous, the voltage and current data are reduced in the same fashion, but the resistivity is called the apparent resistivity. It is the resistivity of a homogeneous earth that would produce the same measurement.

The induced polarization parameters measured depend on whether the system makes use of a time domain or frequency domain waveform (Figs. 7 and 8). For time domain measurements, the maximum value of the voltage during the on cycle, along with the current, can be used to calculate the apparent resistivity. The transient during the off cycle contains the

basic information on induced polarization in the time domain. This transient is specified by its normalized value just after the current is turned off, and by the form and rate of decay. For frequency domain measurements, the basic data are the magnitude and phase of the measured voltage as functions of frequency, from which the amplitude and phase of the apparent resistivity are calculated.

Older analog time domain receivers integrate one or several intervals under the decay curve, at sampling times ranging from about 0.05 to 2.0 s after current shutoff. When the integrated voltage is normalized by the primary voltage (V_o) and the integration time (Δt), the unit of the measurement is given as mV/V (millivolts per volt) and is called the chargeability (M). Another definition of chargeability, the Newmont Standard, does not normalize by the integration time; the units are (mV-s)/V or ms. Since the equivalent integration time of the Newmont Standard is 1 s, normalization by the integration time does not change the numerical value of the chargeability. The Newmont Standard is often written as M331, which refers to a standard pulsed square wave of 3 s on, 3 s off, and an integration time of 1 s. Often measurements are made using different pulse lengths and integration times, which are then reduced to an equivalent M331 using various model-dependent normalization factors (Sumner, 1976).

Analog frequency domain receivers often use two to five frequencies, and many have no current waveform reference, so that phase information is lost. The basic data are then the magnitudes of the apparent resistivity, ρ_1 and ρ_2 at two frequencies, f_1 and f_2, which can be used to calculate percent frequency effect (PFE),

$$PFE = 100\frac{\rho_1 - \rho_2}{\rho_1}, \qquad (43)$$

where ρ_1 is the resistivity at lower frequency.

Modern digital receivers sample the waveform at discrete points in time and store the samples as numbers in the computer memory. Manipulation of the data stored in memory is under program control and, in principle, either time or frequency domain processing can be done. To increase the ratio of signal to noise, multiple cycles are stored and averaged, or stacked, in the memory. Phase information is obtained by using a pair of very accurate, synchronized oscillators at the receiver and transmitter or by using a cable link between the receiver and transmitter.

For the Newmont Standard of chargeability, time domain and frequency domain induced polarization units are related by:

$$M \approx \phi(\text{mrad}) \approx 7PFE/\text{decade of frequency}. \qquad (44)$$

Normally, induced polarization effects produce a positive percent frequency effect, a phase lag (negative phase angle), and a secondary decay voltage with the same sign as the primary (M positive); by convention these are referred to as positive induced polarization effects. Negative induced polarization response (positive phase angle) can be caused by geometric effects with normally polarizable materials and by inductive coupling. Precise measurements are required in induced polarization surveys; even a large induced polarization response of 20 mrad is a phase shift of only 3 degrees.

4.2 Arrays

As noted earlier, arrays used in resistivity surveys in geothermal projects have included Wenner, Schlumberger, dipole-dipole, pole-dipole, and bipole-dipole arrays. If induced polarization surveys are to be conducted, either the pole-dipole or the dipole-dipole array is used in order to minimize electromagnetic coupling. The bipole-dipole array was used extensively after the success Risk et al. (1970) experienced with it at the Broadlands geothermal region in New Zealand. It has been used much less in recent years because the apparent resistivity contour plans obtained with it are complicated, difficult to interpret, and vary significantly with bipole orientation and position. On account of these problems, I will not discuss it further, but will refer the reader to articles by Dey and Morrison (1977), Hohmann and Jiracek (1979), and Frangos and Ward (1980) for evaluations of it. The remaining four arrays are illustrated in Figure 9. Of these, the Wenner array has largely been replaced by the Schlumberger array because the latter is least affected by near-surface inhomogeneities beneath the array (Kunetz, 1966). The dipole-dipole array has largely replaced the pole-dipole array in conductive environments (e.g. geothermal) because it exhibits less electromagnetic coupling.

Table 2 lists eight factors to consider when selecting an array for resistivity or induced polarization surveys. Time domain and frequency domain operations are equivalent but equipment convenience may dictate one or the other. In either domain, one would prefer three decades of spectrum from about 0.1 Hz to 100 Hz for induced polarization surveys in order to permit determination of the polarization spectrum. Table 3 provides an evaluation of the last five factors of Table 2. Where 1 is

entered in a box it indicates the preferred array; where 3 is entered in a box it indicates the least desired array, for that particular factor. Signal-to-noise ratio is superior for the Schlumberger array because the transmitting and receiving electrode pairs are nested. For the same reason, electromagnetic coupling is greatest, i.e. worst, for the Schlumberger array. Double-dipole techniques are always superior to other techniques for lateral resolution of two adjacent steeply dipping bodies. Vertical resolution of adjacent beds in a horizontally layered sequence depends upon the range and density of measurements laterally; the Schlumberger array is best in this regard.

The depths of exploration of resistivity arrays are given by Roy and Apparao (1971) for Schlumberger as 0.125L, and for dipole-dipole as 0.195L, where L is the maximum separation between extreme electrodes (AB for Schlumberger). Thus Schlumberger uses 1.6 times the maximum electrode separation as the dipole-dipole method for the same depth of exploration; this makes it more susceptible to the effects of inhomogeneities offset from the sounding, i.e. lateral effects.

In view of the evaluation of Table 3, it should not be surprising to find: a) that the Schlumberger array is used at many scattered sites within a large region where estimates of the thicknesses and resistivities of assumed horizontal layers are required, while b) that the dipole-dipole array is used on a regular grid of lines where the earth is assumed to be two- and three-dimensionally inhomogeneous.

5.0 PROBLEMS WITH RESISTIVITY AND INDUCED POLARIZATION SURVEYS

5.1 Introduction

As with any geophysical method, application of the resistivity and induced polarization methods encounter problems which can only in part be overcome. Table 4 lists the problems encountered when applying resistivity and/or induced polarization surveys. Each of these problems shall be addressed briefly in the following.

5.2 Natural Field Noise

Natural electric and magnetic fields below 1 Hz are due mainly to the interaction of fields and particles from the sun with the earth's magnetic field; their magnitude depends on solar activity. Above 1 Hz they are primarily due to worldwide thunderstorms. As Figure 10, shows, their amplitude increases rapidly with decreasing frequency below 1 Hz which effectively prevents measurements below about 0.03 Hz. Since electromagnetic coupling is too high above 1 Hz, induced polarization measurements with large arrays are limited to the range 0.03 to 1 Hz. Even in that range, coherent detection and digital high-pass filtering are required to make accurate measurements because of the natural field noise. Stacking, i.e., adding successive transients, is necessary to reduce noise in time domain measurements, but noise rejection is not as good as for coherent detection in the frequency domain.

Commonly, the range of frequencies is extended to 100 Hz or higher, in order to obtain spectra of complex conductivity as shall be described subsequently.

5.3 Cultural Noise

Table 5 lists the sources of cultural noise. Grounded structures

such as fences, powerlines, and pipelines redistribute current from a grounded wire source so that part of the current flows through the cultural feature. Spurious resistivity and induced polarization anomalies arise as a result. In a definitive analysis of the problem, Nelson (1977) found that the only certain means of eliminating such spurious responses is to keep induced polarization transmitting and receiving lines away from grounded structures. However, he was able to do a commendable job in computing the response of a grounded structure for comparison with resistivity phase measured over this structure (Figure 11). Cultural features also can introduce noise into measurements by providing a path for various interfering signals. Of course, strong noise voltages are present in the vicinity of powerlines, requiring filtering at the front end of the receiver. Furthermore, pipelines often carry electrical current for cathodic protection, and this current is a source of noise.

5.4 Effect of Overburden and Other Geologic Noise

Conductive overburden, generally in the form of porous alluvium or weathered bedrock, prevents current from penetrating to the more resistive bedrock. Hence detection of bedrock features is less certain than when overburden is absent.

When the overburden is of irregular resistivity, as illustrated in Figure 12, the *geologic noise* produced by the near-surface features readily obscures the anomaly due to the target in the bedrock.

Anomalies due to geological heterogeneities of no geothermal significance can also obscure, or partly obscure, the anomaly due to a geothermal system.

5.5 Effects of Topography

Much geothermal exploration is done in mountainous terrain where topography can produce spurious resistivity anomalies. In a recent study, Fox et al. (1980) systematically analyzed the effects of topography for the dipole-dipole array using a two-dimensional numerical solution. Figure 13, for example, shows the apparent resistivity anomaly produced by a valley with 30° slopes. The pseudosection is characterized by a central zone of low apparent resistivity flanked by zones of high apparent resistivity. The low is most pronounced when the transmitter and receiver dipoles are on extreme opposite sides of the valley. This example shows that a valley can produce a large, spurious resistivity low which could easily be misinterpreted as evidence for a buried conductor. Similarly, a hill can produce an apparent resistivity high.

Because induced polarization is a normalized measurement, current focusing and dispersion produced by an irregular terrain surface do not significantly affect induced polarization data. Thus if the earth were homogeneous and polarizable, irregular terrain would produce no significant spurious response. However, second-order topographic effects in induced polarization surveys are introduced by variations in distances between surface electrodes and a polarizable body relative to a flat earth.

In general, topographic effects are important where slope angles are 10° or more for slope lengths of one dipole or more. The solution to the problem is to include the topographic surface in numerical models used for interpretation.

5.6 Resolution, Lateral and Vertical

To facilitate vertical resolution, i.e., resolution of the resistivities and thicknesses of horizontally layered media; a wide range and high spatial density of electrode separations is required. Even so, the principle of equivalence (Kunetz, 1966) indicates that substantial ambiguity exists in determining layer thicknesses and resistivities. Resistivity techniques usually provide information on resistivity-thickness products for resistive layers and conductivity-thickness products for conductive layers.

The problem of vertical resolution is illustrated in Figure 14. Superposition of resistivity or induced polarization responses from two or more bodies frequently leads to misinterpretation. Figure 14 shows how the responses of two prisms superpose as they are moved closer together. Each prism is conductive ($\rho_2/\rho_1 = 0.2$), has dimensions 1 width x 4 depth extent x 5 length, and occurs at depth 1. These units are normalized by the dipole length. This case dramatically illustrates the need for sophisticated interpretation of resistivity and induced polarization anomalies: a pseudosection should not be construed as a cross section of the earth. Drilling would be unsuccessful if a hole were spotted over the induced polarization high in the pseudosection in the two cases where the bodies are separated. *Bullseye* pseudosection anomalies such as these often are caused by superposition. When the bodies join, their responses merge into that for a single wide body, as shown in the lower pseudosection of Figure 14.

5.7 Electromagnetic Coupling

The resistivity and induced polarization methods typically use D.C.

formulation which requires that the transmitter and receiver are only coupled resistively. However, when ac is used, which is customary, then electromagnetic coupling between the transmitter and receiver also occurs. This is readily seen in the expression for mutual coupling between a pair of grounded wires (Sunde, 1949).

$$Z = \int_a^b \int_A^B \left[P(r) \cos\theta + \frac{d^2}{dsdS} Q(r) \right] dsdS, \qquad (45)$$

in which

$$Q(r) = \frac{1}{2\pi\sigma r} \text{ is the resistive coupling term,} \qquad (46)$$

and

$$P(r) = -\frac{1}{2\pi\sigma r} \left[\frac{1 - (1 + ikr)e^{-ikr}}{r^2} \right] \qquad (47)$$

is the electromagnetic coupling term. The quantities appearing in these relations are: r is the distance between the electrodes a, b, A, B which terminate the wires, θ is the angle between the wires, σ is the conductivity of the half-space upon which the wires are situated, $k = (-i\sigma\mu\omega)^{1/2}$ is the wavenumber of the half-space, μ is the permeability of the half-space, and ω is angular frequency.

The electromagnetic coupling between the wires increases with frequency, with the lengths ab and AB, with the separation between ab and AB, and with the conductivity of the half-space. Electromagnetic coupling is particularly important to the induced polarization method where one is attempting to measure resistivity as a slowly varying function of frequency, the latter due to electrochemical reactions in the subsurface. As can be seen from the formulation above, electromagnetic coupling is also frequency dependent and it can totally obscure the

induced polarization effects.

Figure 15 illustrates how electromagnetic coupling increases with frequency. Extrapolation of the resistivity phase to zero frequency will eliminate the electromagnetic coupling and leave only the induced polarization effect. Hence an induced polarization survey should utilize several decades of spectrum in order to permit this phase extrapolation.

6.0 INSTRUMENTATION FOR RESISTIVITY AND INDUCED POLARIZATION SURVEYS

Table 6 lists the features of a microprocessor-based resistivity and induced polarization receiver engineered by the Earth Science Laboratory of the University of Utah Research Institute. Its features facilitate coherent detection which are necessary for enhancing signal-to-noise ratio and for recognizing and removing electromagnetic coupling. The high pass filtering before stacking significantly improves signal to noise ratio as SanFilipo and Hohmann (1982) have established. The automatic gain ranging and self-potential buckout features speed observations as does the use of dual channels.

A transmitter of equally modern design does not exist but has been outlined by engineers of the Earth Science Laboratory in Table 7.

7.0 APPLICATIONS OF INDUCED POLARIZATION IN GEOTHERMAL EXPLORATION

7.1 Roosevelt Hot Springs, Utah, USA

Roosevelt Hot Springs thermal area, located in west-central Utah, covers approximately 32 sq km on the western margin of the Mineral Mountains. The thermal reservoir occurs within fractured Precambrian gneisses and Tertiary granitic rocks of the Mineral Mountains pluton (Sibbett and Nielson, 1980). At least ten rhyolite domes occur along the crest of the Mineral Mountains, representing igneous activity between 0.5 and 0.8 million years ago. A deep-seated magma body related to this young rhyolitic volcanism is a possible heat source for the present geothermal system (Smith and Shaw, 1975).

Hot spring deposits in the Roosevelt thermal area consist of opaline sinter. The alluvium is cemented by this siliceous sinter, locally. Alluvium, plutonic rocks of granite to granodiorite composition, and amphibolite facies have been altered by acid-sulfate water to alunite and opal at the surface, and to kaolinite, alunite, montmorillonite, and muscovite to a depth of 60m. Marcasite and pyrite occur below the water table at about 30m. Deeper alteration sampled to a depth of 2.25 km consists of muscovite, chlorite, calcite, K-feldspar, albite, and epidote with pyrite and sparse chalcopyrite. Alteration in producing and non-producing wells occurs mainly along faults and fractures that mark past and present fluid channels (Parry et al., 1978).

Chu et al. (1979) report on an attempt to define by induced polarization the geothermal productive zone at the Roosevelt Hot Springs thermal area. Apparent resistivity amplitude and phase data were gathered with a coherent detection system at frequencies between 32 Hz

and 1/256 Hz. The resulting field data, an example of which is shown in Figure 16, exhibit no unequivocal resistivity phase anomalies between stations 3 and 12 where the fracture dominated geothermal reservoir exists. There is a tendency toward slightly higher values centered on station 12, but these could be accounted for by increasing overburden to the east and west of station 12. On the other hand, there is a definite increase of resistivity phase with depth throughout the section depicted in Figure 16. We attribute this to electromagnetic coupling (even though the frequency used was 1/4 Hz) or to the expected response of a virtually unpolarized overburden over a slightly polarized earth. Values of phase of about 5 to 15 mrad are normal background in induced polarization surveys. The spectrum of resistivity phase for one field observation is shown in Figure 17. It would appear that electromagnetic coupling is the cause of the phase anomaly and that it is asymptoting to zero at about 10^{-2} Hz, below which we know that noise badly contaminates the data. The residual resistivity phase at 10^{-2} Hz is about 8 mrad, a value consistent with expected background.

Two explanations for these low values of polarization are evident. First, because the polarizable alteration minerals, i.e. clays and pyrite, are largely restricted to fractures and faults, the volume of polarizable materials is small and hence not detectable. Second, the faults and fractures containing brine of 7000 ppm total dissolved solids carry most of the current so that little current passes through the polarizable materials. On a laboratory scale, individual altered core samples were polarizable, as expected. We conclude that the induced polarization method is not viable at this geothermal site.

7.2 Other Areas

An application of induced polarization at a second site in Utah, the Cove Fort-Sulphurdale thermal area, also resulted in only background values for resistivity phase (Ross, 1979).

In both of the areas tested in Utah the geothermal reservoirs are characterized by porosity due to widely spaced fractures and faults. In those reservoirs where significant intergranular porosity is present, or where fractures are pervasive, the thermal fluids may cause ubiquitous alteration and hence ubiquitous distribution of polarizable minerals. This is certainly true of the fossil geothermal systems known as porphyry copper deposits in the mining industry. For this reason, the induced polarization method should be tested further in geothermal exploration. In this respect, it is interesting to note that Zohdy et al. (1973) report an induced polarization anomaly at the Mud Volcano area in Yellowstone National Park, USA, while Risk (1975a,b) suggests that he observed the induced polarization effect at the Broadlands geothermal field, New Zealand.

8.0 BASIC PRINCIPLES AND PROBLEMS WITH S.P. SURVEYS

8.1 Introduction

Corwin and Hoover (1979) recently published a very useful summary of the use of the self-potential method in geothermal exploration.

Self-potentials in geothermal areas arise in electrokinetic, thermoelectric, and to a minor extent in electrochemical sources (Corwin and Hoover, 1979; Sill, 1981; Sill, 1982a,b,c). Sill (1982b) has established that the electrochemical contribution is unlikely to exceed 10 mV. Tending to obscure the electrokinetic and thermoelectric anomalies of geothermal origin is noise arising in telluric currents, electrode drift, topography, variations in soil moisture, cultural stray currents, vegetation potentials, and electrokinetic potentials from shallow, moving groundwater. With care in surveys, one can usually reproduce measurements to ± 5 mV but noise of short spatial wavelength will remain and often is as large as ± 10 mV.

8.2 Survey Procedures

In principle, self-potential surveys are very simple: two non-polarizing electrodes, a length of wire, and a D.C. voltmeter are all the equipment needed to perform a survey. However, much attention must be paid to details if the reproduceability of ± 5 mV, noted above, is to be achieved. Two methods of moving the electrodes along the traverse line are used; they are *leapfrog* and *long wire* methods. In the former, the back electrode is leapfrogged past the forward electrode for each move. Only a short wire is required. In the long wire method, the back electrode is left fixed and the forward electrode is moved farther and farther away. A long length of wire is then required. The relative

advantages and disadvantages of the two methods will be discussed in the following section.

8.3 Noise in Self-Potential Surveys

Table 8 lists the sources of noise encountered in self-potential surveying, each of which will be addressed in the following.

8.3.1 Telluric currents

Time-varying voltages induced in the earth by the geomagnetic field, of frequencies within the passband of the voltmeter, may reach several hundred mV/km over resistive terrain (Keller and Frischknecht, 1966). These time-varying voltages constitute noise which inhibits repeatability of a measurement of the d.c. self-potentials. The magnitude of this noise is proportional to the separation between the two electrodes and accordingly is largest for the *long wire* method. If telluric noise is dominant, then the *leapfrog* method is preferred.

8.3.2 Electrode drift

A voltage will be measured across an electrode pair if either or both of the electrodes are not in equilibrium. Departure from zero electrode potential will occur if the electrolyte in the non-polarizing electrode is diluted or contaminated by groundwater or if there is a temperature differential between the two. These effects will vary with time, moisture content of the soil, and ambient temperature. Repeated checks of drift must be made periodically by placing both measuring electrodes in a bath of electrolyte solution and connecting them in order to establish equlibrium. Leapfrog surveys usually resulted in irregular electrode drift so that long

wire surveys are preferred where electrode drift is the dominant source of noise.

8.3.3 Topography

Topographic relief will distort self-potentials and this effect must be taken into account in interpretation of field data. Another topographic effect is due to the movement of shallow groundwater. More negative potentials are sometimes correlated with an increase in elevation with observed gradients as large as -6 mv/m (Hoover, 1981).

8.3.4 Variations in soil moisture

As noted by Corwin and Hoover (1979), variations in soil moisture often give rise to self-potential variations, with the electrode in the wetter soil usually becoming more positive. Watering of electrodes to improve electrical contact can produce the same effect, but even worse, electrokinetic potentials are generated as the water moves through the soil. Electrode watering should be avoided for self-potential surveys in geothermal areas because the geothermal anomalies frequently are small, so that reducing noise to a minimum becomes essential.

8.3.5 Cultural noise

Table 9 lists some sources of cultural noise encountered when performing S.P. surveys. All of them can lead to time varying potentials, while corrosion potentials and potentials from corrosion protection systems additionally will produce spurious anomalies. Results from self-potential surveys in a developing or developed geothermal field will be quite different from results obtained

before well casings were installed. Figure 18 illustrates, dramatically, the self-potential anomaly due to a drill casing nine months after installation. The anomaly is due to a corrosion potential and increased with time after the placement of the casing.

8.3.6 Vegetation potentials

Trees, shrubs, and grasses produce potentials which are commonly of order 10 mV. A common technique used to reduce this noise, and noise due to varying soil moisture, involves making five measurements in a star about each observation point. Four readings are offset about 3 m north, south, east, and west of the central point. The five readings are then averaged.

8.3.7 Electrokinetic potentials from moving non-thermal water

Potentials generated by the flow of nonthermal surface and subsurface water, i.e. electrokinetic potentials, constitute a noise source in goethermal exploration, and may be a major cause of topographic noise (Corwin and Hoover, 1979).

8.4 Modeling of Self-Potential Data

In a series of articles, Sill (1981, 1982a,b,c) has developed a numerical modeling capability for computing self-potential anomalies due to electrokinetic, thermoelectric, and electrochemical sources. The modeling algorithm utilizes induced current sources which result from the divergence of the convective current. The convective current is driven, in turn, by a primary flow, either heat or fluid.

Figure 19 shows the self potential anomaly due to a point pressure source S_p located at a contact between rock types of differing

resistivities ρ. The fluid impermeability ρ_p is homogeneous and the voltage coupling coefficient C and resistivity change across the contact. The anomaly is monopolar, i.e. symmetric, and increases negatively as the resistivity contrast ρ_2/ρ_1 changes across the contact.

While the pressure anomaly for the model of Figure 19 is monopolar, a dipolar anomaly can be produced if the overburden has a very large permeability so that there is vertical flow across horizontal boundaries (Fig. 20). The anomaly shape changes dramatically with resistivity contrast at the vertical contact. For the same two models, a point temperature source at the contact produces dipolar anomalies whether or not the overburden is present. Monopolar temperature anomalies can be produced with horizontal contacts.

9.0 THE MONROE-RED HILL HOT SPRINGS CASE HISTORY

9.1 Introduction

As an example of the integration of electrical surveys in a geothermal exploration strategy, the Monroe-Red Hill hot springs case history is presented in the following.

The Monroe-Red Hill hydrothermal system occupies the eastern flank of the central Sevier River Valley, immediately east of the town of Monroe, Utah, USA. The springs issue from the Sevier fault which is a major west-dipping normal fault marking the western termination of the Sevier Plateau against the alluvial fill of the Sevier River Valley.

The region surrounding the Monroe-Red Hill hydrothermal system has been the object of geological, geochemical and geophysical studies by the University of Utah on behalf of the U.S. Department of Energy. The first detailed studies of these hot springs (Parry et al., 1976; Miller, 1976) were concerned with the geochemistry and alteration mineralogy of the system and provide valuable constraints on the origin and history of the thermal waters. During the summer of 1977, and extending into 1978, a detailed geophysical study consisting of heat flow, dipole-dipole resistivity, ground magnetics and precision gravity (Halliday, 1978; Mase et al., 1978) was conducted to assess the resource potential of the hydrothermal system. The detailed study covered a 40 km^2 area along the Sevier Fault near the Monroe and Red Hill hot springs.

9.2 Geology

Mase et al. (1978) summarize the geology, geochemistry, and geophysics of this prospect and in the following we shall draw freely from their article. The central Sevier River Valley is an alluvial

filled intermontaine valley bounded on the east by the Sevier Plateau and on the west by the Pavant Range. The Sevier Plateau, with its gently sloping summit, more nearly resembles the Colorado Plateau to the east, while the Pavant Range with its many structural features is more characteristic of the Basin and Range Province.

Tertiary volcanics are the dominant rocks of the area. The Monroe and Red Hill hot springs are located near the northern edge of the Marysvale volcanic field, where extensive and prolonged volcanism occurred from middle to late Tertiary. The volcanics range in composition from basalt to rhyolite and in age from Oligocene to Pliocene. The volcanic rocks lie upon sedimentary rocks that vary in age from Jurassic to Oligocene, depending upon location.

The Bullion Canyon volcanics comprise the dominant rock type in the Monroe-Red Hill area and are Miocene in age. They are comprised of pyroclastics in the lower part, overlain by thick porphyritic latite flows and breccias with an upper member consisting of basaltic andesite flows.

Intrusive igneous bodies of Miocene age are associated with the Bullion Canyon volcanics. The intrusions primarily consist of stocks ranging from monzonitic to granitic composition. The nearest stock to the Monroe-Red Hill system is located at Monrovian Park, three miles to the southeast. The stock is about one mile in diameter and is typical of other Miocene intrusives that have invaded the volcanics.

High angle normal faulting is the dominant structural feature of the transition zone between the Colorado Plateau and the Basin and Range

Province and is responsible for many of the topographic features as well. The Sevier fault zone from which the hot springs issue is mostly buried by alluvium and has been inferred in most localities to be near the western termination of the Sevier Plateau against the alluvial fill of the Sevier River valley.

Hot and warm springs occur at changes in the surface trace of the Sevier fault. Presumably these are the only places where permeable conduits exist in the fault zone through which water may rise to the surface.

The lack of Pleistocene and Quaternary volcanism suggests that a magmatic intrusion is an unlikely explanation for the heat source. The geology and geochemistry indicates that deep circulation, storage and heating within a reservoir, due to a normal Basin and Range heat flow with subsequent discharge to the surface through the Sevier fault zone, is more likely. Figure 21 represents an idealized geologic cross section through the Monroe-Red Hill system depicting the Nuggett member of the Navajo sandstone as the hot reservoir. The recharge of the Nuggett sandstone probably occurs in the highlands of the Sevier Plateau, through available fractures and faults in the overlying volcanic and sedimentary cover.

9.3 Geochemistry

Na-K-Ca and silica geothermometers indicate temperatures of last wall rock equilibration of 187°C and 104°C respectively, for the thermal fluids. The Na-K-Ca geothermometer may be considered unreliable because the hot spring water may have acquired its salinity from evaporites within the Arapien shale. From geochemistry, Parry et al. (1976)

determined that the spring waters are most likely a mixture of a hot saline component and a cool component that is chemically similar to surface water in the area. A mixing model, based on the measured silica content of the warm water and the warm water enthalpy, indicate a mixture of 62% hot water at 118°C and 38% cold water at 10°C. In normal Basin and Range terrain with a heat flow of 80 mW m^{-2}, this temperature is reached between 2.0 and 4.0 km, depending on rock type and thermal conductivity. The aquifer that constitutes the hot fluid reservoir may be the Jurassic Navajo sandstone which is generally permeable and lies beneath the volcanic cover. The location of mixing between the hot and cold waters is speculative, but may take place at the intersection of the Sevier fault with the basaltic andesite flows of the Bullion Canyon volcanics, the contact between the Jurassic Arapien shale and Bullion Canyon volcanics,or the limestone beds contained within the Arapien shale.

9.4 Geophysics

9.4.1 Heat flow and geothermal gradient

A heat flow map of Figure 22 the Monroe-Red Hill area was constructed on the basis of temperature measurements in eleven holes drilled to depths ranging from 40 to 90 m. An empirical correlation between heat flow and resistivity, shown as an inset in Figure 22, was used as a guide in contouring heat flow. Values of heat flow greater than 2000 mWm^{-2} were observed. Thermal conductivities were measured from core or chips and combined with the temperature measurements to compute the heat flow. Mase et al. (1978) have estimated that the combined conductive and convective heat flow from the Monroe-Red Hill Hot Springs area is about 8 MW (thermal).

Figure 23 illustrates temperature gradients and temperature versus depth contours for the profile of thermal gradient holes drilled across the Red Hill Hot Springs. The isotherms of Figure 23 are upwarped under the discharge vent. Similar data is shown in Figure 24 for Monroe Hot Springs. The data sets of Figures 23 and 24 confirm the conceptual model of Figure 20.

9.4.2 Resistivity

Fourteen resistivity profiles across the Sevier fault were used to construct a 100 m dipole-dipole first separation apparent resistivity contour map, Figure 25, from which inferences about the flow of the subsurface hot springs may be drawn. The map effectively outlines the trace of the Sevier fault and contains an elongate zone of low resistivity (<10 Ω-m) associated with the discharging thermal fluids along the Sevier fault and the intense alteration accompanying the hot springs. All of the surface geothermal manifestations in the Monroe-Red Hill area are contained within the 10 Ω-m contour line. This zone defines the Monroe-Red Hill system as an elongate zone .5 km wide and 3 km long which may consist of two plumes, one centered over the Monroe Hot Springs mound and the other over Red Hill Hot Springs. The arm of low resistivity projecting northwest from Red Hill is interpreted as leakage of cooling thermal fluids through the alluvium.

A two-dimensional transmission surface algorithm was used to model the resistivity data in east-west cross sections. Figure 26 contains observed and computed pseudosections plus the corresponding earth model for a dip of the low-resistivity fault zone of 60°

west. The fit between observed and computed pseudosections was worse for this model than for one in which the dip of the fault was vertical. Hence the model of Figure 21, which includes a dip near vertical, is endorsed. It is important to note that no element of the model of Figure 26 is deeper than 400 m. Our experience suggests that a maximum depth of exploration for the dipole-dipole resistivity method is about 2a where a is the dipole length, provided dipole lengths lie in the range 100 m to 300 m. For dipole lengths of 1 km to 6 km, which we have used, the depth of exploration can be considerably less if the overburden is conductive.

9.4.3 Self-potential

Sill (1981) modeled the Red Hill Hot Springs thermal profile of Figure 23 along with the corresponding resistivity profile in order to predict temperatures in the subsurface and to compare observed and modeled self-potential contours in plan view. Figure 27 shows the two-dimensional distribution of thermal resistivity ρ_T, coupling coefficient C, and electrical resistivity ρ used in the model calculations. Figure 27 also shows the observed and modeled two-dimensional temperature distributions along the profile; the agreement is excellent. Figure 28 compares the observed and modeled self-potential plan view data; once again the agreement is excellent. It is evident that the modeling technique of Sill (1981) is powerful insofar as it provides estimates of the temperature distribution and promises to give quantitative information on fluid flow in the subsurface.

10.0 CONCLUSION

Of the electrical methods discussed herein, the resistivity and self-potential methods have been established as essential to geothermal exploration. Where tested by the Earth Science Laboratory, the induced polarization method has not been successful presumably because polarizable materials constitute only a small fraction of the volume of low electrical resistivity under study. However, Risk (1975a) and Zohdy et al. (1973) appear to have had success with it. Further study of the induced polarization method in geothermal environments is warranted because of its unique capability for distinguishing between zones of low resistivity caused by brines and those caused by the presence of clay minerals.

This article has concentrated on the fundamentals and problems of the three methods discussed, with only one integrated field case history presented. For similar integrated case histories developed by the Earth Science Laboratory, the reader is referred to Ward et al. (1978) and Ross et al. (1982) for Roosevelt Hot Springs, Utah, USA, and to Hulen (1978), Fox (1978a,b,) for Coso Hot Springs, California, USA. The introduction contains numerous references to electrical methods case histories appearing in the general literature.

11.0 ACKNOWLEDGEMENTS

This report was delivered at the U.N. University, Reykjavik, Iceland, in September, 1982. I am grateful to Dr. Ingvar Fridleifsson of Orkustofnun for inviting me to participate in this activity. Joan Pingree typed the manuscript, Doris Cullen supervised preparation of the illustrations while Carl Ruscetta provided technical editing; we are indebted to all of them.

12.0 REFERENCES

Arnorsson, S., Bjornsson, A., Gislason, G., and Gudmundsson, G., 1975, Systematic exploration of the Krisuvik high-temperature area, Reykjanes Peninsula, Iceland: Second U. N. Symposium on the Development and Use of Geothermal Resources, Proc., v. 2, p. 853-864.

Baudu, R., Bernhard, J., Georgel, J. M., Griveau, P., Rugo, R., 1980, Application of D. C. Dipolar methods in the Upper Rhinegraben: Advances in European and Geothermal Research, Dordrecht, Holland, D. Reidel Co., p. 823-832.

Banwell, C. J. and Macdonald, W. J. P., 1965, Resistivity surveying in New Zealand thermal areas: Eighth Commonwealth Mining and Metallurgical Congress, Australia and New Zealand, New Zealand Section, p. 1-7.

Beyer, H. J., Morrison, H. F., and Dey, A., 1975, Electrical exploration of geothermal systems in the Basin and Range valleys of Nevada: Second U. N. Symposium on the Development and Use of Geothermal Resources, Proc., p. 889-894.

Bibby, H. M., 1977, The apparent resistivity tensor: Geophysics, v. 42, p. 1258-1261.

Bibby, H. M., and Risk, G. F., 1973, Interpretation of dipole-dipole resistivity surveys using a hemispheroidal model: Geophysics, v. 38, p. 719-736.

Campbell, R. E., 1977, Geophysical Drill Hole Casing Anomalies *in* Workshop on Mining Geophysics: Univ. of Utah, Dept. Geol. and Geophys., Report on NSF Grant AER76-80802, p. 257-268.

Campbell, W. H., 1967, Geomagnetic pulsations, *in* S. Matsushita and W. H. Campbell, eds., Physics of geomagnetic phenomena: New York, Academic Press, p. 822-909.

Chu, J. J., Sill, W. R., and Ward, S. H., 1979, Induced polarization measurements at Roosevelt Hot Springs thermal area, Utah: Univ. of Utah, Dept. Geol. and Geophys., Report IDO/78-1701.a.2.4.1, DOE/DGE contract EG-78-C-07-1701, 34 p.

Corwin, R. F., and Hoover, D. B., 1979, The self-potential method in geothermal exploration: Geophysics, v. 44, p. 226-245.

Dey, A. and Morrison, H. F., 1977, An analysis of the bipole-dipole method of resistivity surveying: Geothermics, v. 6, p. 47-81.

Doicin, D., 1976, Quadripole-quadripole arrays for direct current resistivity measurements-model studies: Geophysics, v. 41, p. 79-95.

Duba, A. and Heard, H. C., 1980, Effect of hydration on the electrical conductivity of olivene: EOS Transactions, 61, p. 404.

Fox, R. C., 1978a, Dipole-dipole resistivity survey of a portion of the Coso Hot Springs KGRA, Inyo County, California: Univ. of Utah Res. Inst., Earth Sci. Lab., Report IDO/77.5.6, DOE Contract EY-76-S-07-1601, 21 p.

Fox, R. C., 1978b, Low-altitude aeromagnetic survey of a portion of the Coso Hot Springs KGRA, Inyo County, California: Univ. of Utah Res. Inst., Earth Sci. Lab., Report IDO/77.5.7, DOE Contract EY-76-S-07-1601, 19 p.

Fox, R. C., Hohmann, G. W., Killpack, T. J., and Rijo, L., 1980, Topographic effects in resistivity and induced polarization surveys: Geophysics, v. 43, p. 144-172.

Frangos, W., and Ward, S. H., 1980, Bipole-dipole survey at Roosevelt Hot Springs thermal area, Beaver County, Utah: Univ. of Utah Res. Inst./Earth Science Laboratory, Report DOE/ID/12079-15, 41 p.

Garcia, D. S., 1975, Geoelectric study of the Cerro Prieto geothermal area, Baja California: Second U. N. Symposium on the Development and Use of Geothermal Resources, Proc., v. 2, p. 1009-1012.

Grahame, D. C., 1947, The electrical double layer and the theory of electrocapillarity: Chem. Rev., v. 41, p. 441-501.

Grim, R. E. 1953, Clay mineralogy: New York, McGraw-Hill Book Co., Inc., 384 p.

Gupta, M. L., Singh, S. B., and Rao, B. V., 1975, Studies of direct current resistivity in the Puga geothermal field, Himalayas, India: Second U. N. Symposium on the Development and Use of Geothermal Resources, Proc., v. 2, p. 1029-1036.

Halliday, M. E., 1978, Gravity and ground magnetic surveys in the Monroe and Joseph Known Geothermal Resource Areas and surrounding region, south-central Utah: Univ. Utah Dept. Geol. and Geophys., M.S. Thesis.

Harrington, R. F., 1961, Time-harmonic electromagnetic fields, New York, McGraw-Hill Book Co., Inc. 480 p.

Harthill, H., 1978, A quadripole resistivity survey of the Imperial Valley, California: Geophysics, v. 43, p. 1485-1500.

Hatherton, T., Macdonald, W. J. P., and Thomson, G. E. K., 1966, Geophysical methods in geothermal prospecting in New Zealand: Bull. Volcanology, p. 485-497.

Hohmann, G. W. and Jiracek, G. R., 1979, Bipole-dipole interpretation with three-dimensional models: Univ. of Utah Res. Inst./Earth Science Laboratory, Report DOE/ET/28392-29, 20 p.

Hohmann, G. W., and Ward, S. H., 1981, Electrical methods in mining geophysics: Econ. Geol., 75th Anniversary Volume, 1981, p. 806-828.

Hoover, D. B., 1981, Self-potential investigations at Mt. Hood, Oregon, paper presented at the Self-Potential Workshop, Golden, Colorado, March 3-4, 1981.

Hulen, J. B., 1978, Geology and alteration of the Coso geothermal area Inyo County, California: Univ. of Utah Res. Inst., Earth Sci. Lab., Report IDO/78-1701.b.4.1., DOE Contract EG-78-C-07-1701, 28 p.

Jiracek, G. R., and Smith, C., 1976, Deep resistivity investigations at two known geothermal resource areas (KGRAs) in New Mexico: Radium Springs and Lightning Dock: New Mexico Geol. Soc. Spec. Pub. No. 6, p. 71-76.

Jiracek, G. R., Smith, C., Dorn, G. A., 1975, Deep geothermal exploration in New Mexico using electrical resistivity: Second U. N. Symposium on the Development and Use of Geothermal Resources, Proc., p. 1095-1102.

Keller, G. V., and F. C. Frischknecht, 1966, Electrical methods in geophysical prospecting: New York, Pergammon Press, 517 p.

Keller, B. V., Furgerson, R., Lee, C. Y., Harthill, N., Jacobson, J. J., 1975, The dipole mapping method: Geophysics, v. 40, p. 451-472.

Kittel, C., 1953, Introduction to solid state physics: New York, John Wiley and Sons, Inc., 617 p.

Klein, D. P., Kauahikaua, J. P., 1975, Geoelectric-geothermal exploration on Hawaii Island, preliminary results: report, Hawaii Institute of Geophysics.

Kunetz, G., 1966, Principles of direct current resistivity prospecting: Geopublication Associates Geoexploration Mon., Ser, No. 2, 103 p.

Lebedev, E. B. and Khitarov, N. I., 1964, Dependence on the beginning of melting of granite and the electrical conductivity of its melt on high water vapor pressure: Geokhimija, 3, p. 195-201.

Macdonald, W. J. P. and Muffler, L. J. P., 1972, Recent geophysical exploration of the Kaweran geothermal field, North Island, New Zealand: New Zealand J. Geol. and Geophys., v. 15, p. 303-317.

Mase, C., Chapman, D. S., and Ward, S. H., 1978, Geophysical study of the Monroe-Red Hill Geothermal System: Univ. Utah Dept. Geol. & Geophys., Rept. IDO/76-1601-77-17.

McNitt, J. R., 1975, Summary of United Nations geothermal exploration experience, 1965 to 1975: Second, U. N. Symposium on the Development and Use of Geothermal Resources, Proc., p. 1137-1134.

Meidav, T. and Furgerson, R., 1972, Resistivity studies of the Imperial Valley geothermal area, California: Geothermics, v. 1, p. 47-62.

Miller, C. D., 1976, Alteration and geochemistry of the Monroe Known Geothermal Resource Area: Univ. Utah, Dept. Geol. & Geophys., M.S. Thesis.

Moskowitz, B., and Norton, D., 1977, A preliminary analysis of intrinsic fluid and rock resistivity in active hydrothermal systems: J. Geophys. Res., v. 82, p. 5787-5795.

Nelson, P. H., 1977, Induced polarization effects from grounded structures: Geophysics, v. 42, p. 1241-1253.

Parry, W. T., Benson, N. L., and Miller, C. D., 1976, Geochemistry and hydrothermal alteration at selected Utah hot springs, Rpt. Dept. Geol. and Geophys., Univ. of Utah, NSF Grant GI-43741, Vol. 3.

Parry, W. T., Bryant, N. L., Dedolph, R. E., Ballantyne, J. M., Ballantyne, G. H., Rohrs, D. T., and Mason, J. L., 1978, Hydrothermal alteration at the Roosevelt Hot springs thermal area, Utah: Univ. of Utah, Dept. Geol. and Geophys., Report IDO/78-1701.a.1.1, DOE/DGE contract EG-78-C-07-1701, 29 p.

Patella, D., Quarto, R., and Tramacere, A., 1980, Dipole-dipole study of the Travale geothermal field: Advances in European Geothermal Research, Dordrecht, Holland, D. Reidel Co., p. 833-842.

Patella, D., Rossi, A., Tramacere, A., 1979, First results of the application of the dipole electrical sounding method in the geothermal area of Travale-Radicondoli (Tuscany): Geothermics, v. 8, p. 111-134.

Pelton, W. H. , Ward, S. H., Hallof, P. G., Sill, W. R., and Nelson, P. H., 1978, Mineral discrimination and removal of inductive coupling with multifrequency IP: Geophysics, 43, p. 588-609.

Pridmore, D. F., Hohmann, G. W., Ward, S. H., and Sill, W. R., 1981, An investigation of finite-element modeling for electrical and electromagnetic data in three dimensions: Geophysics, v. 46, p. 1009-1024.

Rai, C. S., and Manghnani, M. H., 1978, Electrical conductivity of basalts to 1550°C: *in* ed. H. J. B. Dick, Proc. of Chapman Conference on Partial Melting in the Earth's Upper Mantle, Oregon, Dept. Geol. and Min. Ind., Bull. 96, p. 219-232.

Razo, A., Arellano, F., and Fouseca, H., 1980, CFE resistivity studies at Cerro Prieto: Geothermics, v. 9, p. 7-14.

Risk, G. F., 1975a, Monitoring the boundary of the Broadlands geothermal field, New Zealand: Second U. N. Symposium on the Development and Use of Geothermal resources, Proc., p. 1185-1190.

Risk, G. F., 1975b, Detection of buried zones of fissured rock in geothermal fields using resistivity anisotropy measurements: Second U. N. Symposium on the Development and Use of Geothermal Resources, Proc., p. 1191-1198.

Risk, G. F., Macdonald, W. J. P., and Dawson, G. B., 1970, D. C. Resistivity surveys of the Broadlands geothermal region, New Zealand: Geothermics, Spec. Issue 2, v. 2, p. 287-294.

Ross, H. P., Nielson, D. L., and Moore, J. N., 1982, Roosevelt Hot Springs geothermal system, Utah - Case Study: Bull. AAPG, vol. 66, no. 7, p. 879-902.

Ross, H. P., 1979, Numerical modeling and interpretation of dipole-dipole resistivity and IP profiles, Cove Fort-Sulphurdale KGRA, Utah: Univ. Utah Res. Inst., Earth Sci. Lab., Rept. DOE/ET/28392-37, 39 p.

Roy, A., and Apparao, A., 1971, Depth of investigation in direct current resistivity prospecting: Geophysics, v. 36, p. 943-959.

SanFilipo, W. A., and Hohmann, G. W., 1982, Computer simulation of low-frequency electromagnetic data acquisition: Univ. of Utah Res.Inst./Earth Science Laboratory, Report ESL 62, 33 p.

Shankland, T. J., and Waff, H. S., 1977, Partial melting and electrical conductivity anomalies in the upper mantle: J. Geophys. Res., v. 82, p. 5409-5417.

Sibbett, B. S., and Nielson, D. L., 1980, Geology of the Central Mineral Mountains, Beaver County, Utah: Univ. of Utah Res. Inst., Earth Sci. Lab. Rep. No. 33, DOE/DGE contract DE-AC07-78ET28392, 42 p.

Sill, W. R., 1981, Self potential modeling from primary flows: Univ. of Utah, Dept. Geol. and Geophys., Report DOE/ID/12079-42, 28 p.

Sill, W. R., 1982a, Self-potential effects due to hydrothermal convection, velocity cross-coupling: Univ. of Utah, Dept. of Geol. and Geophys., DOE/DGR Report No. DOE/ID/12079-68.

Sill, W. R., 1982b, Diffusion Coupled (Electrochemical) Self-potential effects in geothermal Areas: Univ. of Utah, Dept. of Geol. and Geophys., DOE/DGR Report No. 12-79-73.

Sill, W. R., 1982c, A model for the cross-coupling parameters of rocks: Univ. of Utah, Dept. of Geol. and Geophys., DOE/DGR Report No. DOE/ID/12079-69.

Smith, R. L., and Shaw, H. R., 1975, Igneous related geothermal systems: in D. E. White and D. L. Williams, eds., Assessment of Geothermal Resources of the United States - 1975, U. S. Geol. Surv. Circ. 726, p. 58-83.

Souto, J. M., 1978, Oahu geothermal exploration: Geothermal Resources Council, Trans., v. 2, p. 605-607.

Stanley, W. D., Jackson, D. B., Zohdy, A. A. R., 1976, Deep electrical investigations in the Long Valley geothermal area, California: J. Geophys. Res. v. 81, p. 810-820.

Stratton, J. A., 1941, Electromagnetic Theory, New York, McGraw-Hill Book Co., Inc., 616 p.

Sumner, J. S., 1976, Principles of induced polarization for geophysical exploration: New York, Elsevier Scientific Publishing Co., 277 p.

Sunde, E. D., 1949, Earth conduction effects in transmission systems: New York, D. Van Nostrand Co. Inc., 373 p.

Tripp, A. C., Ward, S. H., Sill, W. R., Swift, C. M., and Petrick, W. R., 1978, Electromagnetic and Schlumberger resistivity sounding in the Roosevelt Hot Springs KGRA: Geophysics, v. 43, p. 1450-1469.

Ward, S. H., and Fraser, D. C., 1967, Conduction of electricity in rocks, *in* Mining Geophysics, Vol. II: Tulsa, Soc. Exploration Geophysicists, p. 197-223.

Ward, S. H., and Sill, W. R., 1976, Dipole-dipole resistivity surveys, Roosevelt Hot Springs KGRA: Univ. of Utah, Dept. Geol. and Geophys., Final Report v. 2, NSF Grant GI-4374, 29 p.

Ward, S. H., Parry, W. T., Nash, W. P., Sill, W. R., Cook, K. L., Smith, R. B., Chapman, D. S., Brown, F. H., Whelan, J. A., and Bowman, J. R., 1978, A summary of the geology, geochemistry, and geophysics of the Roosevelt Hot Springs thermal area, Utah: Geophysics, v. 43, p. 1515-1542.

Williams, P. L., Mabey,D. R., Zohdy, A. A. R., Ackermann, H., Hoover, D. B., Pierce, K. L., and Oriel, S. S., 1975, Geology and geophysics of the southern Raft River Valley geothermal area, Idaho, USA: Second U. N. Symposium on the Development and Use of Geothermal Resources, Proc., p. 1273-1282.

Wilt, M. J., Goldstein, N. E., and Razo, A. 1980, LBL resistivity studies at Cerro Prieto: Geothermics, v. 9, p. 15-26.

Zohdy, A. A. R., Anderson, L. A., and Muffler, L. J. P., 1973, Resistivity, self-potential, and induced polarization surveys of a vapor-dominated geothermal system: Geophysics, v. 38, p. 1130-1144.

13.0 FIGURE CAPTIONS

Fig. 1. Schematic representation of ions adsorbed on clay particle (after Ward and Fraser, 1967).

Fig. 2. (a) Hypothetical anomalous ion distribution near a solid-liquid interface; (b) Corresponding potential distribution (after Ward and Fraser, 1967).

Fig. 3. Circuit analog of interfacial impedance (after Ward and Fraser, 1967).

Fig. 4. Simplified representation of mineralized rock, (a) and the corresponding equivalent circuit (b) and (c) equivalent circuit of all mineralized rocks (after Ward and Fraser, 1967).

Fig. 5. Simplified analog circuit model of rock. (a) Elementary circuit, (b) frequency response of elementary circuit, (c) transient response of elementary circuit, and (d) a generalization of the elementary circuits.

Fig. 6. Depiction of ions in a pore space forming an ion concentration barrier which creates membrane polarization: (a) Pore path before application of an electric potential, (b) Pore path after application of a potential (after Ward and Fraser, 1967).

Fig. 7. Transmitted and received waveforms in the frequency domain (after Hohmann and Ward, 1981).

Fig. 8. Transmitted and received waveforms in the time domain (after Hohmann and Ward, 1981).

Fig. 9. Depiction of the common arrays used in resistivity and induced polarization surveys.

Fig. 10. Generalized spectrum of natural magnetic fields (after Campbell, 1967).

Fig. 11 Phase lag in mrad. due to a power line and a computed model using the grounded impedance measured on one of the power poles. The computed model half-space parameters were 50 Ω m and 3 mrad. The grounding impedances were 100 Ω m at 160 mrad., with 11 grounds in the calculation. One of the grounds is 5 m from the center IP electrode. (After Nelson, 1977).

Fig. 12. Resistivity pseudosections over an earth model consisting of a contact between two rock types, a massive sulfide body at the contact, and an irregular overburden (after Pridmore et al., 1981).

Fig. 13. Apparent resistivity anomaly due to a two-dimensional valley with 30° slopes (after Fox et al., 1980).

Fig. 14. Resolution of adjacent bodies. Superposition of induced polarization responses due to two prisms: width = 1a, depth extent 4a, length = 5a, depth = 1a, ρ_2/ρ_1 = 0.2. Dipole length is a. Anomaly contours is B_2 (%) which is the fraction of the intrinsic polarization of 100 given to the bodies. B_2 (%) can therefore represent PFE, M, or ϕ (after Hohmann and Ward, 1981).

Fig. 15. Phase spectra for various dipoles and various spacings from IP survey in conductive terrane, Northern Territory, Australia. (Data by Phoenix Geophysics Ltd.).

Fig. 16. Resistivity phase pseudosection at 1/4 Hz for Line 2200 N, Roosevelt Hot Springs, 300 m dipoles (after Chu et al., 1979).

Fig. 17. Resistivity amplitude and phase versus log frequency for 300 m dipoles, Roosevelt Hot Springs (after Chu et al., 1979).

Fig. 18. Self-potential profile prior to and nine months subsequent to placement of casing in a drill hole (after Campbell, 1977).

Fig. 19. Surface voltage for a point pressure source S_p located at a vertical contact. ρ_p is fluid resistivity, ρ is electrical resistivity, while C^p is the voltage coupling coefficient (after Sill, 1981).

Fig. 20. Surface voltage for a point pressure source S_p located at a vertical contact covered by overburden. ρ_p is fluid resistivity, ρ is electrical resistivity, while C is the voltage coupling coefficient (after Sill, 1981).

Fig. 21. Generalized geologic cross section of the Sevier Fault near Monroe, Utah, U. S. A. (after Mase et al., 1978).

Fig. 22. Monroe-Red Hill heat flow map (after Mase et al., 1978).

Fig. 23. Temperature-depth curves and isotherm cross section for Red Hill Hot Springs (after Mase et al., 1978).

Fig. 24. Temperature-depth curves and isotherm cross section for Monroe Hot Springs (after Mase et al., 1978).

Fig. 25. Dipole-dipole first separation apparent resistivity contour map of the Monroe-Red Hill geothermal system (after Mase et al., 1978).

Fig. 26. Electrical resistivity model with 60° dip on the Sevier Fault, Monroe Hot Springs (after Mase et al., 1978).

Fig. 27. (Top) Physical properties used to model the data at Red Hill Hot Springs ρ_T is thermal resistivity, ρ is electrical resistivity, C is voltage coupling coefficient.
(Bottom) Comparison of the observed and calculated temperatures at Red Hill Hot Springs (after Sill, 1981).

Fig. 28. Comparison of the observed and modeled self-potential anomaly at Red Hill Hot Springs.

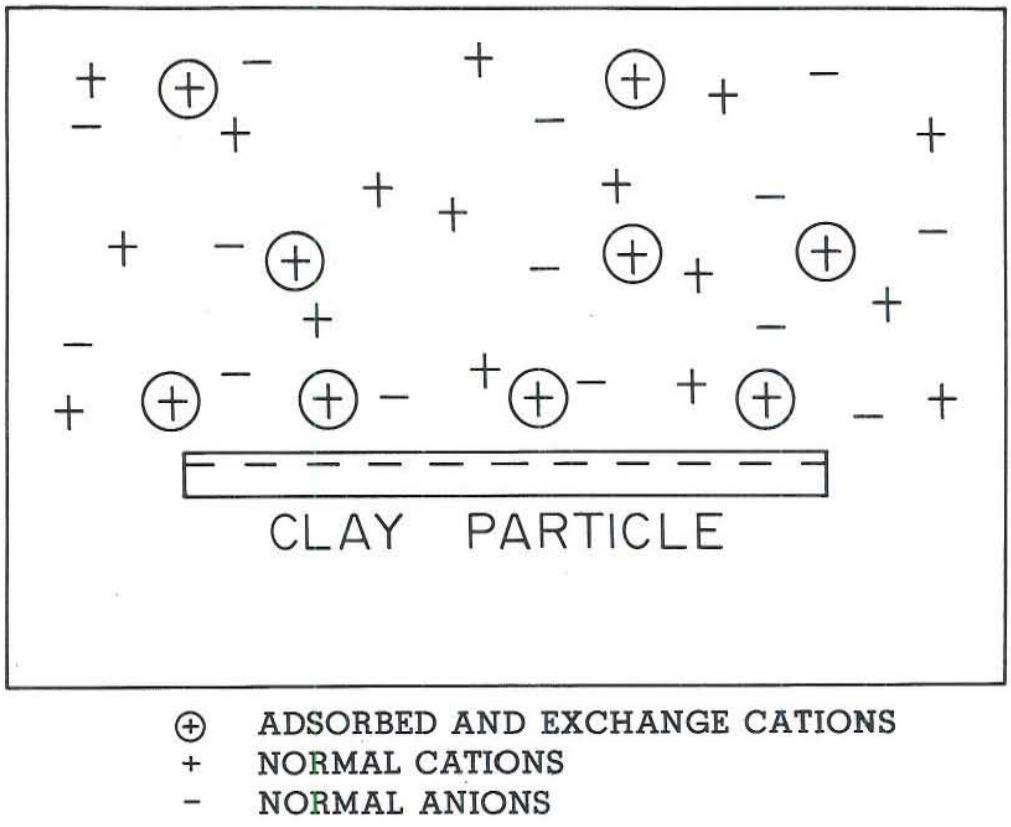

Fig. 1. Schematic representation of ions adsorbed on clay particle (after Ward and Fraser, 1967).

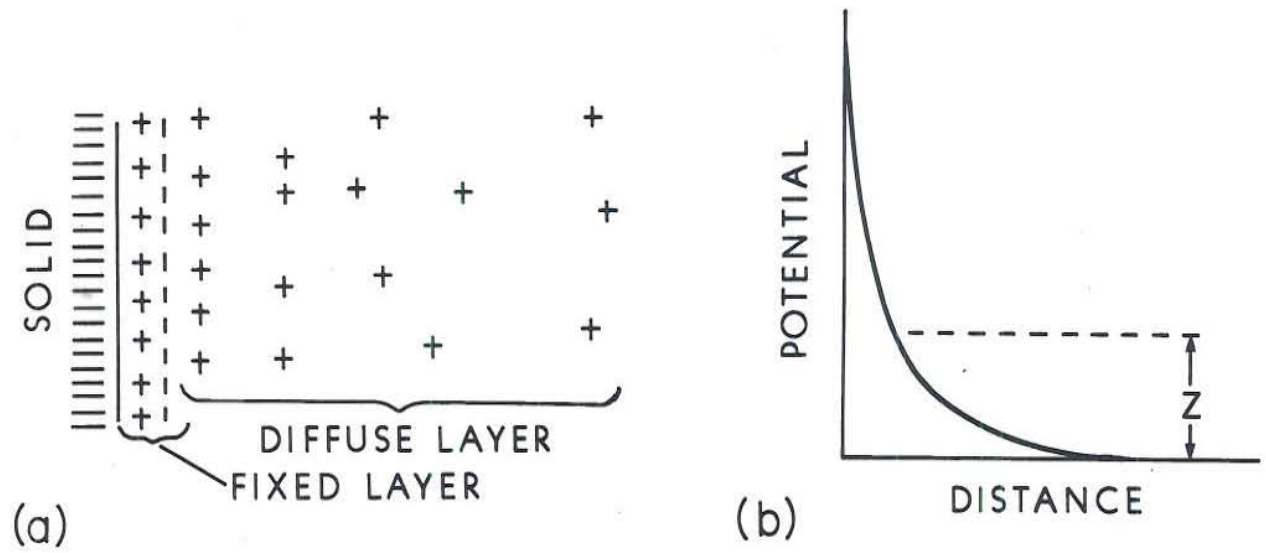

Fig. 2. (a) Hypothetical anomalous ion distribution near a solid-liquid interface; (b) Corresponding potential distribution (after Ward and Fraser, 1967).

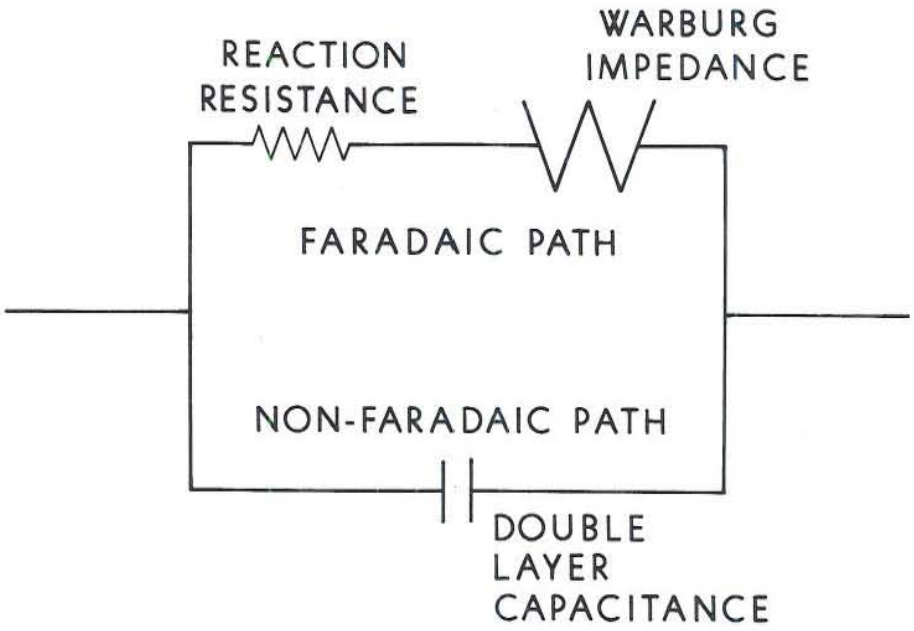

Fig. 3. Circuit analog of interfacial impedance (after Ward and Fraser, 1967).

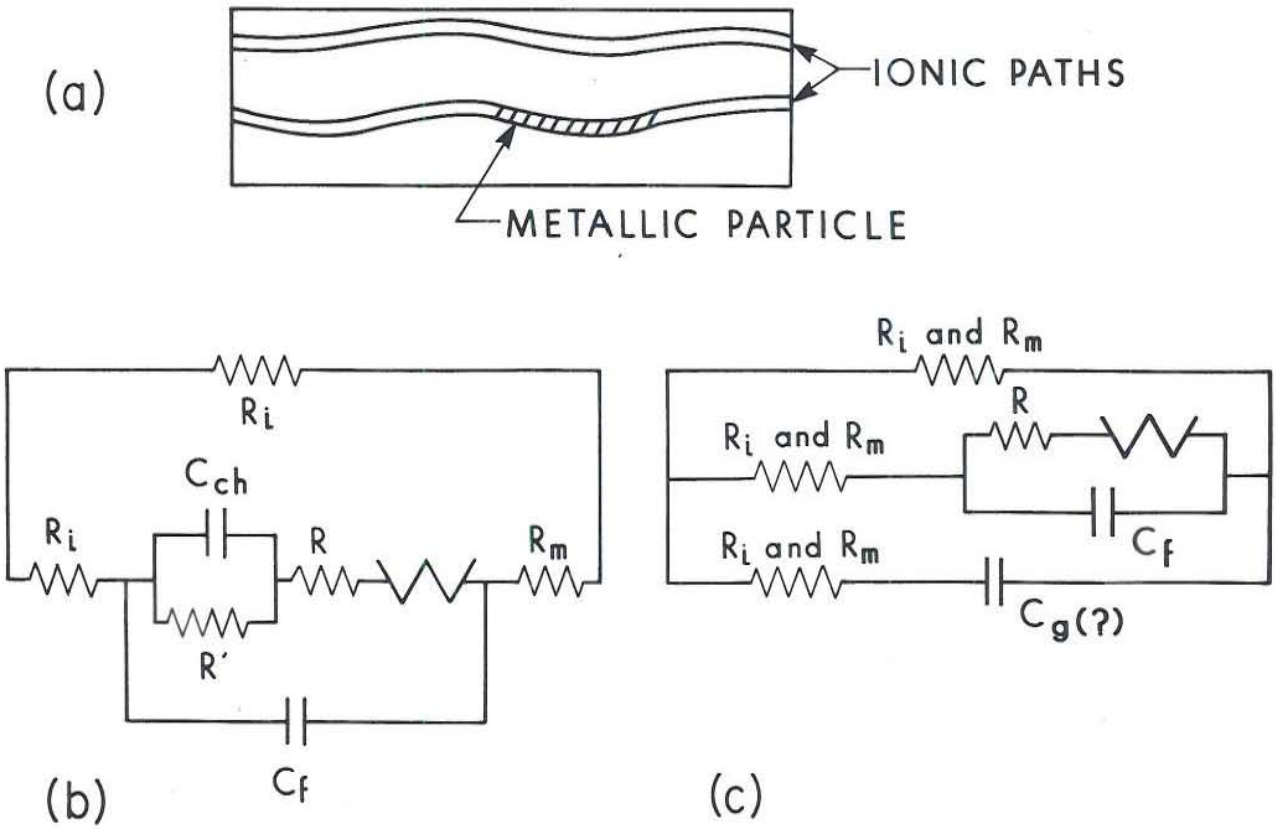

Fig. 4. Simplified representation of mineralized rock, (a) and the corresponding equivalent circuit (b) and (c) equivalent circuit of all mineralized rocks (after Ward and Fraser, 1967).

ANALOG CIRCUIT MODEL OF ROCK

a) ELEMENTARY CURCUIT

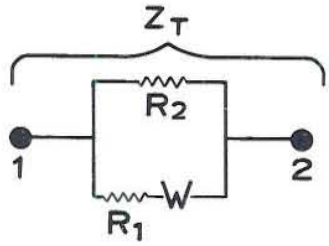

$$Z_2 = \frac{R_1 + W}{1 + \frac{R_1}{R_2} + \frac{W}{R_2}}$$

b) FREQUENCY RESPONSE - SINE WAVE EXCITATION

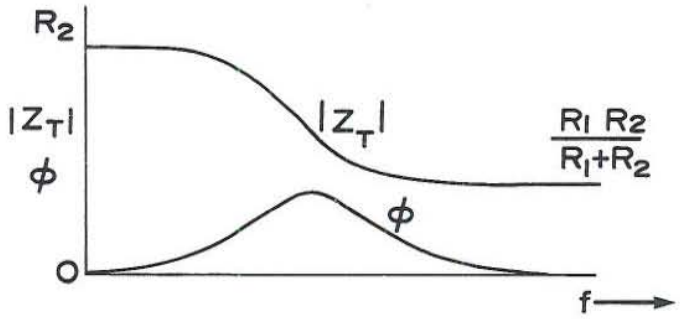

c) TRANSIENT RESPONSE SQUARE WAVE EXCITATION

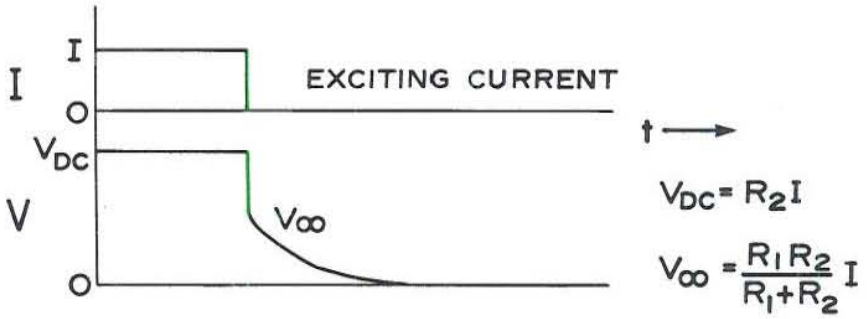

Fig. 5. Simplified analog circuit model of rock. (a) Elementary circuit, (b) frequency response of elementary circuit, (c) transient response of elementary circuit.

MEMBRANE POLARIZATION

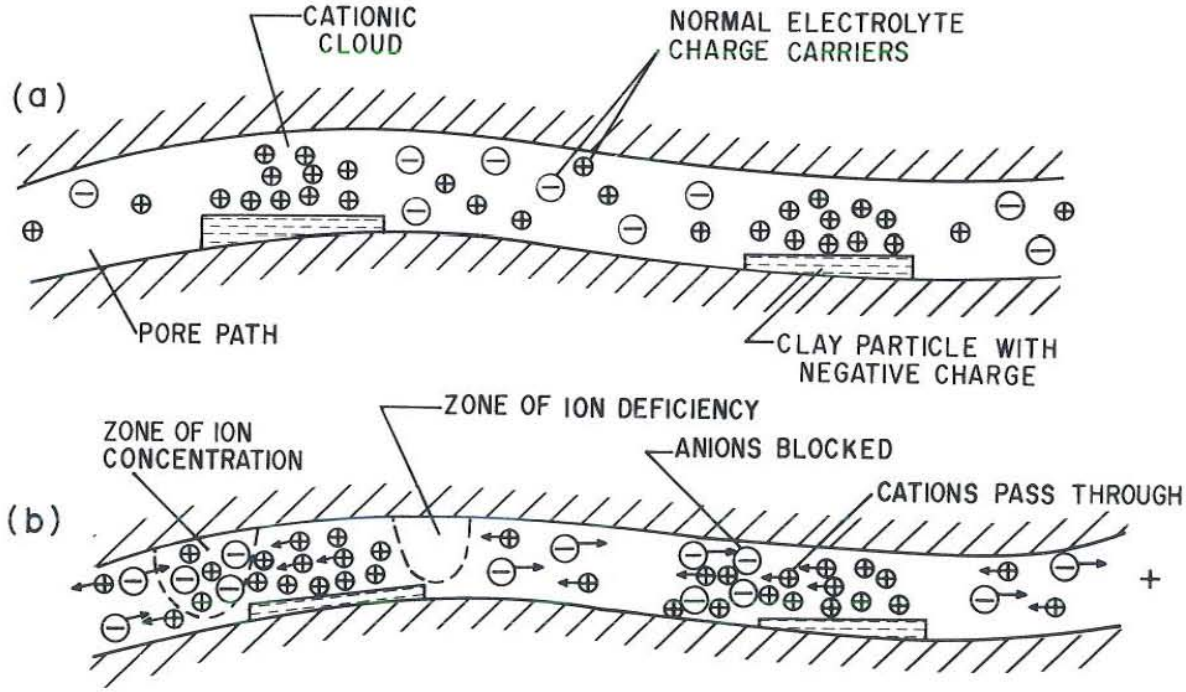

Fig. 6. Depiction of ions in a pore space forming an ion concentration barrier which creates membrane polarization: (a) Pore path before application of an electric potential, (b) Pore path after application of a potential (after Ward and Fraser, 1967).

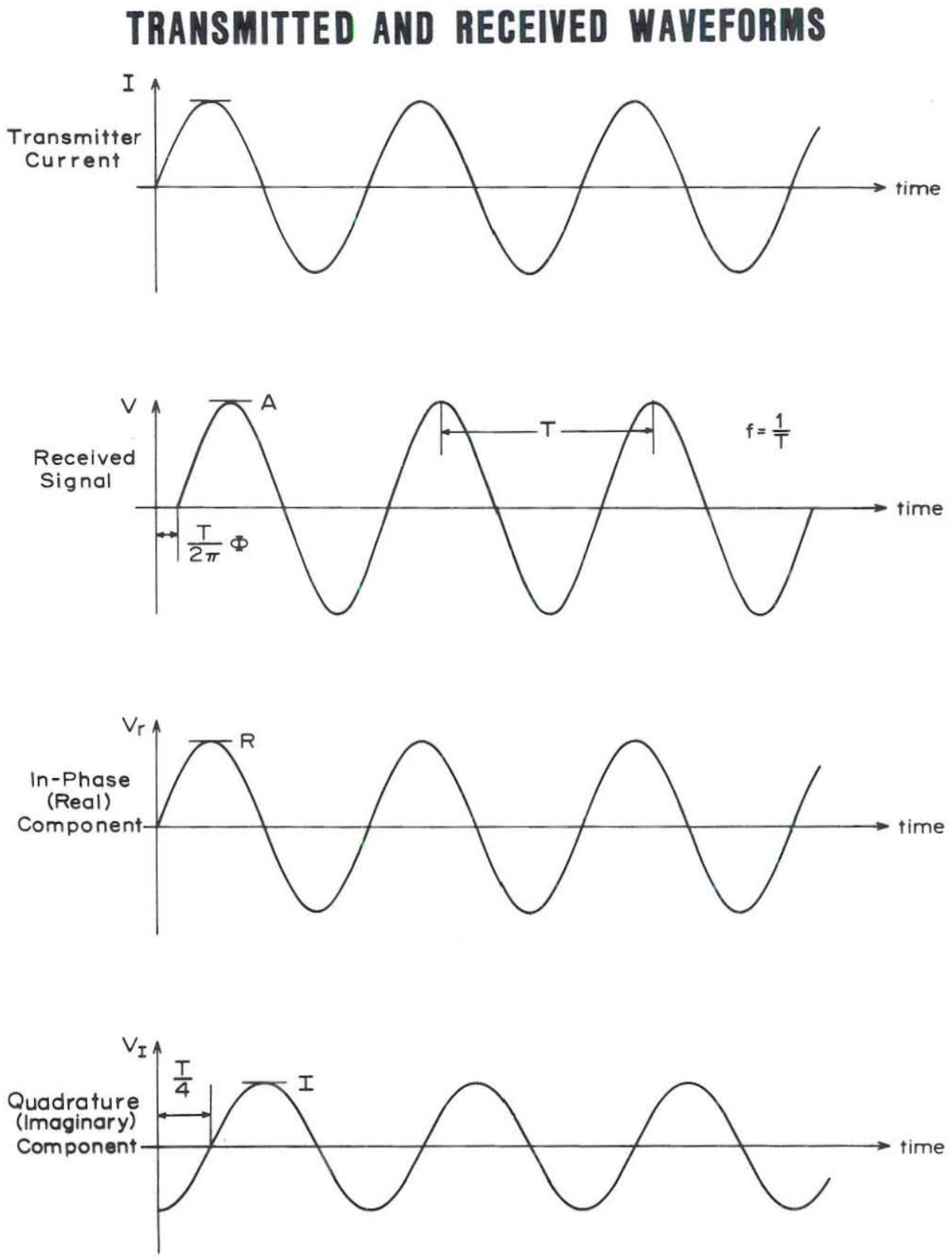

Fig. 7. Transmitted and received waveforms in the frequency domain (after Hohmann and Ward, 1981).

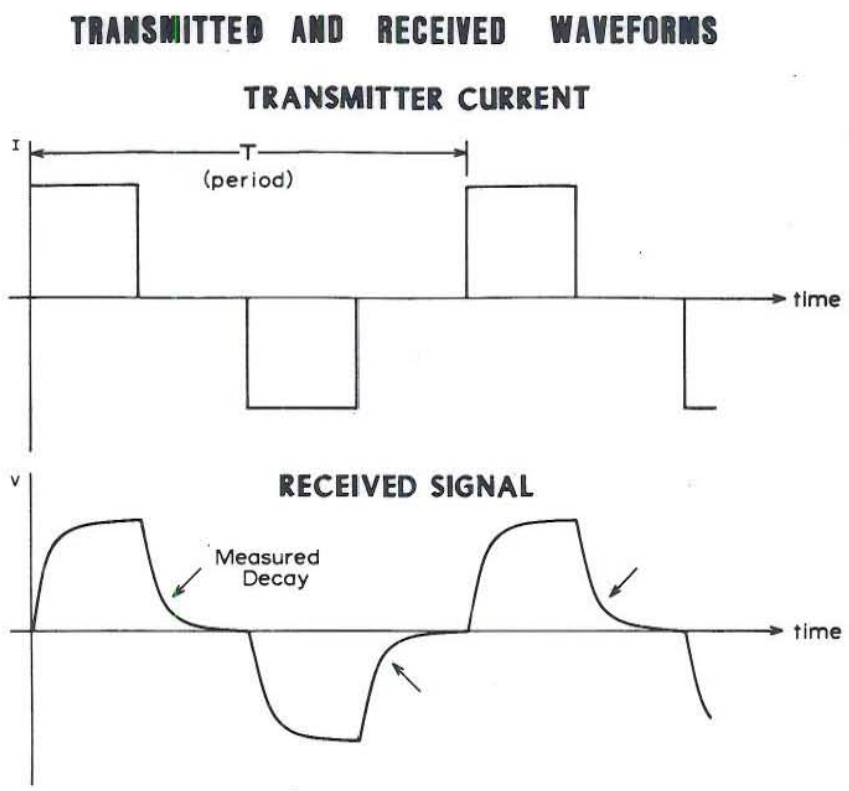

Fig. 8. Transmitted and received waveforms in the time domain (after Hohmann and Ward, 1981).

RESISTIVITY AND IP ARRAYS

ARRAY	GEOMETRY	K	DISPLAY	USE
WENNER	a a a	$2\pi a$	ρa vs a	SOUNDING
SCHLUMBERGER	na a na	$\pi n(n+1)a$	ρa vs $(n+1/2)a$	SOUNDING
POLE-DIPOLE	na a	$2\pi n(n+1)a$	ρa vs n	SOUNDING-PROFILING
DIPOLE-DIPOLE	a na a	$\pi n(n+1)(n+2)a$	ρa vs n	SOUNDING-PROFILING

Fig. 9. Depiction of the common arrays used in resistivity and induced polarization surveys.

NATURAL MAGNETIC FIELD SPECTRUM

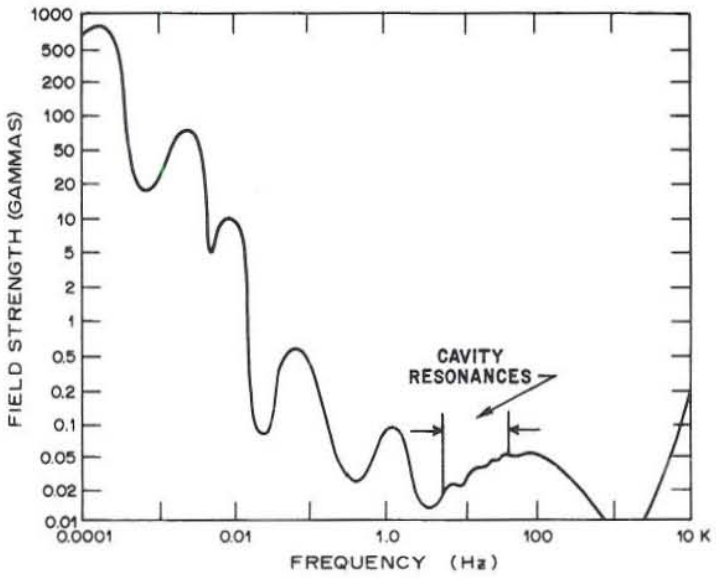

Fig. 10. Generalized spectrum of natural magnetic fields (after Campbell, 1967).

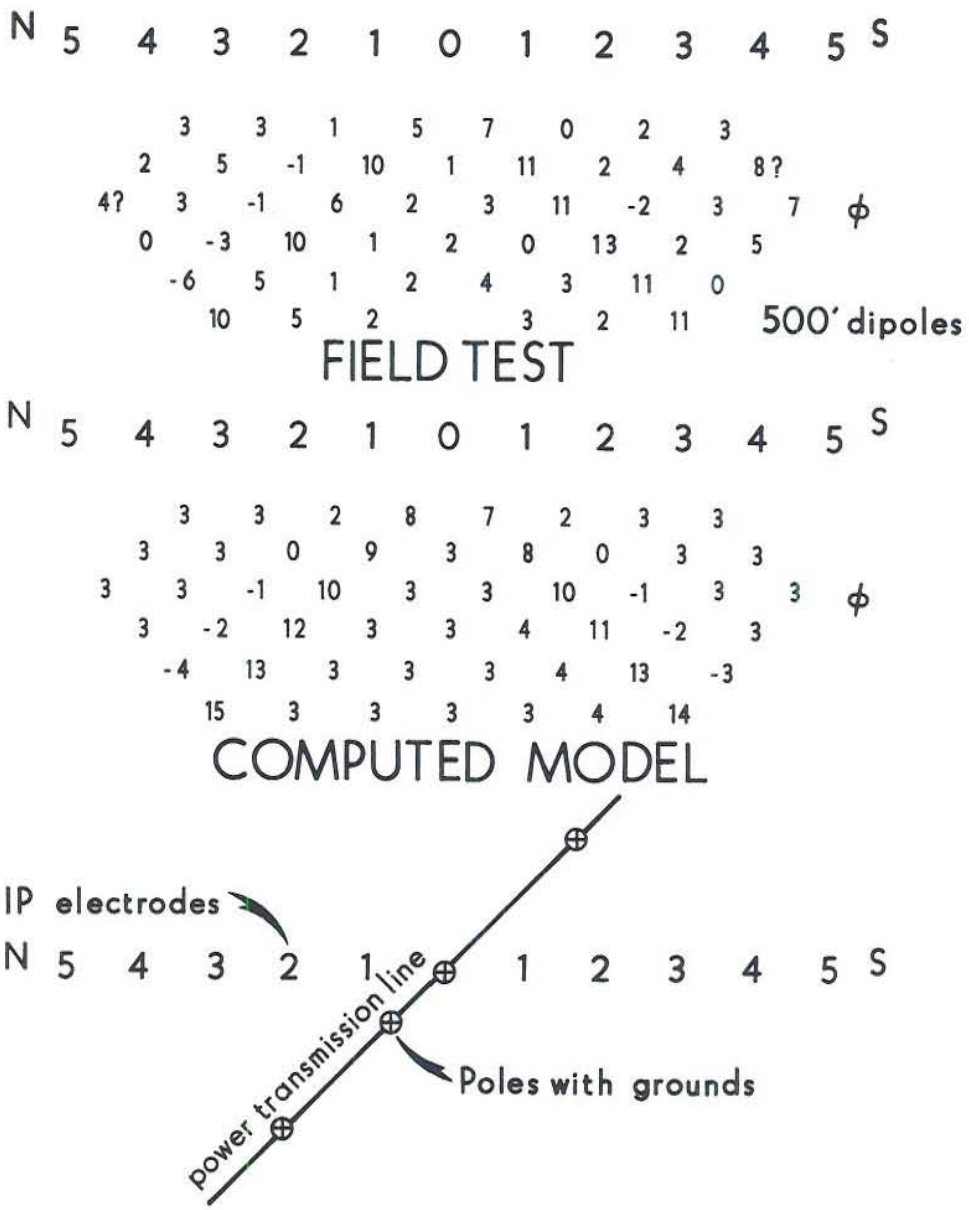

Fig. 11 Phase lag in mrad. due to a power line and a computed model using the grounded impedance measured on one of the power poles. The computed model half-space parameters were 50 Ω m and 3 mrad. The grounding impedances were 100 Ω m at 160 mrad., with 11 grounds in the calculation. One of the grounds is 5 m from the center IP electrode. (After Nelson, 1977).

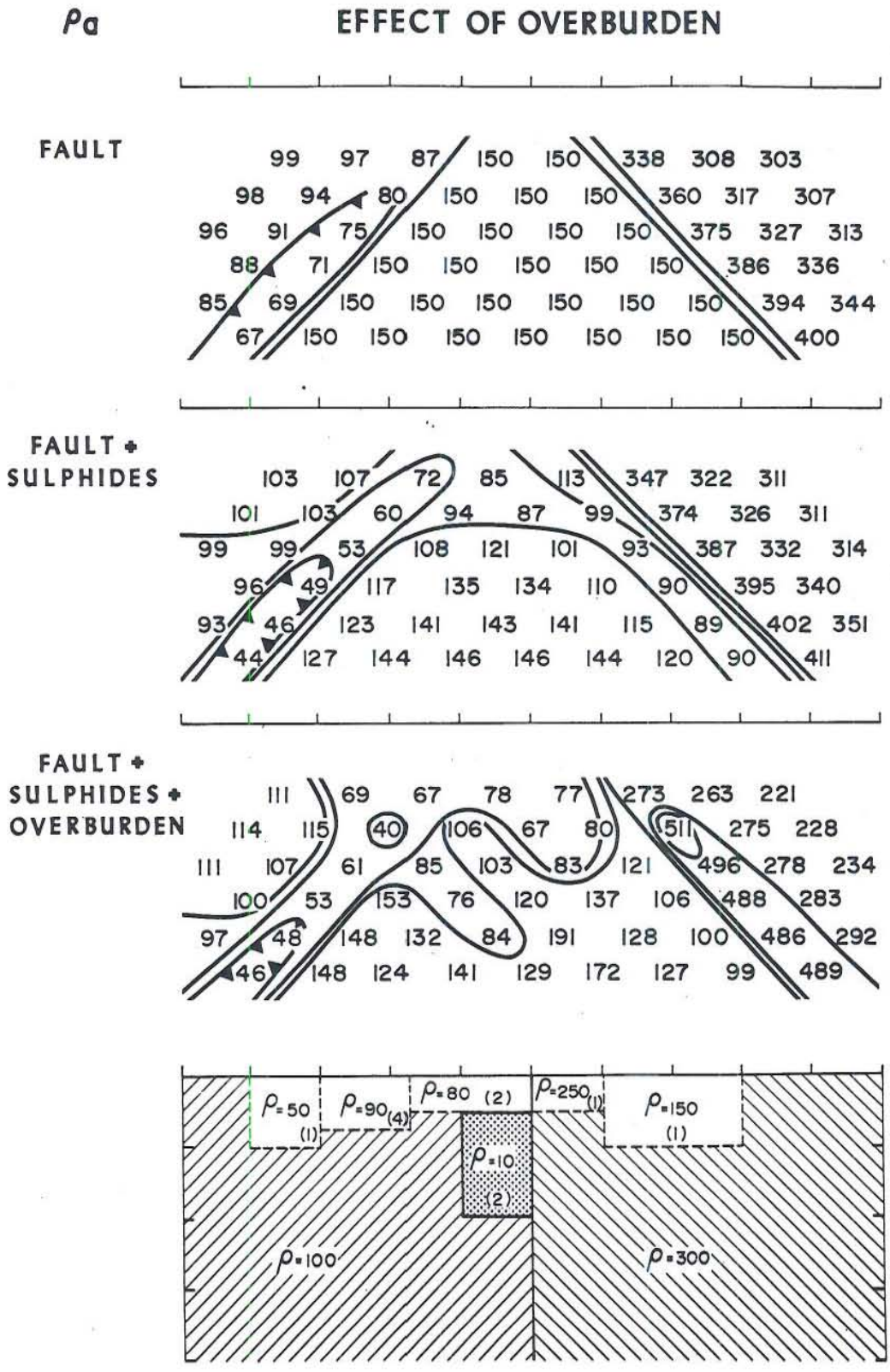

Fig. 12. Resistivity pseudosections over an earth model consisting of a contact between two rock types, a massive sulfide body at the contact, and an irregular overburden (after Pridmore et al., 1981).

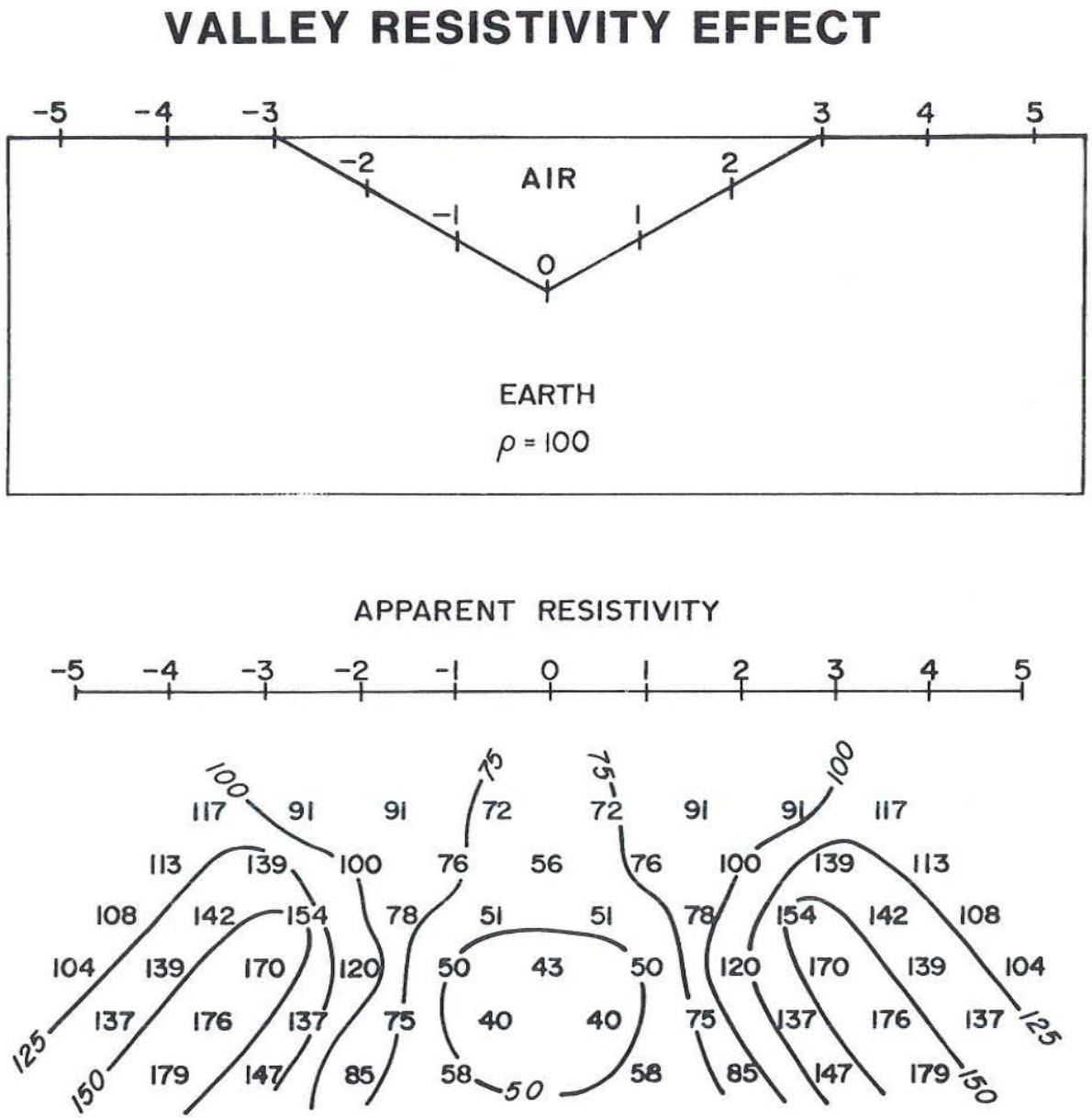

Fig. 13. Apparent resistivity anomaly due to a two-dimensional valley with 30° slopes (after Fox et al., 1980).

EFFECT OF MULTIPLE BODIES

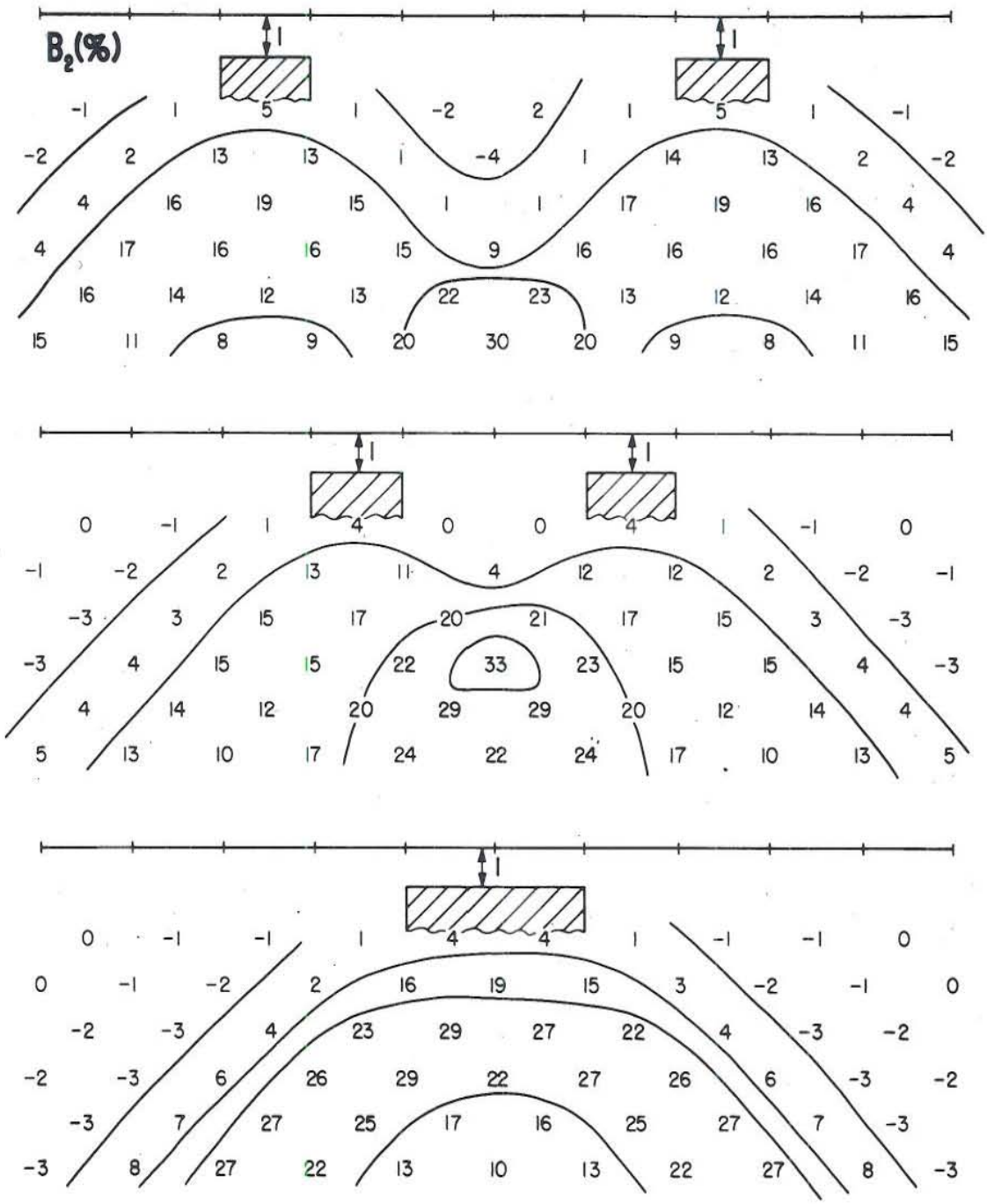

Fig. 14. Resolution of adjacent bodies. Superposition of induced polarization responses due to two prisms: width = 1a, depth extent 4a, length = 5a, depth = 1a, ρ_2/ρ_1 = 0.2. Dipole length is a. Anomaly contours is B_2 (%) which is the fraction of the intrinsic polarization of 100 given to the bodies. B_2 (%) can therefore represent PFE, M, or ϕ (after Hohmann and Ward, 1981).

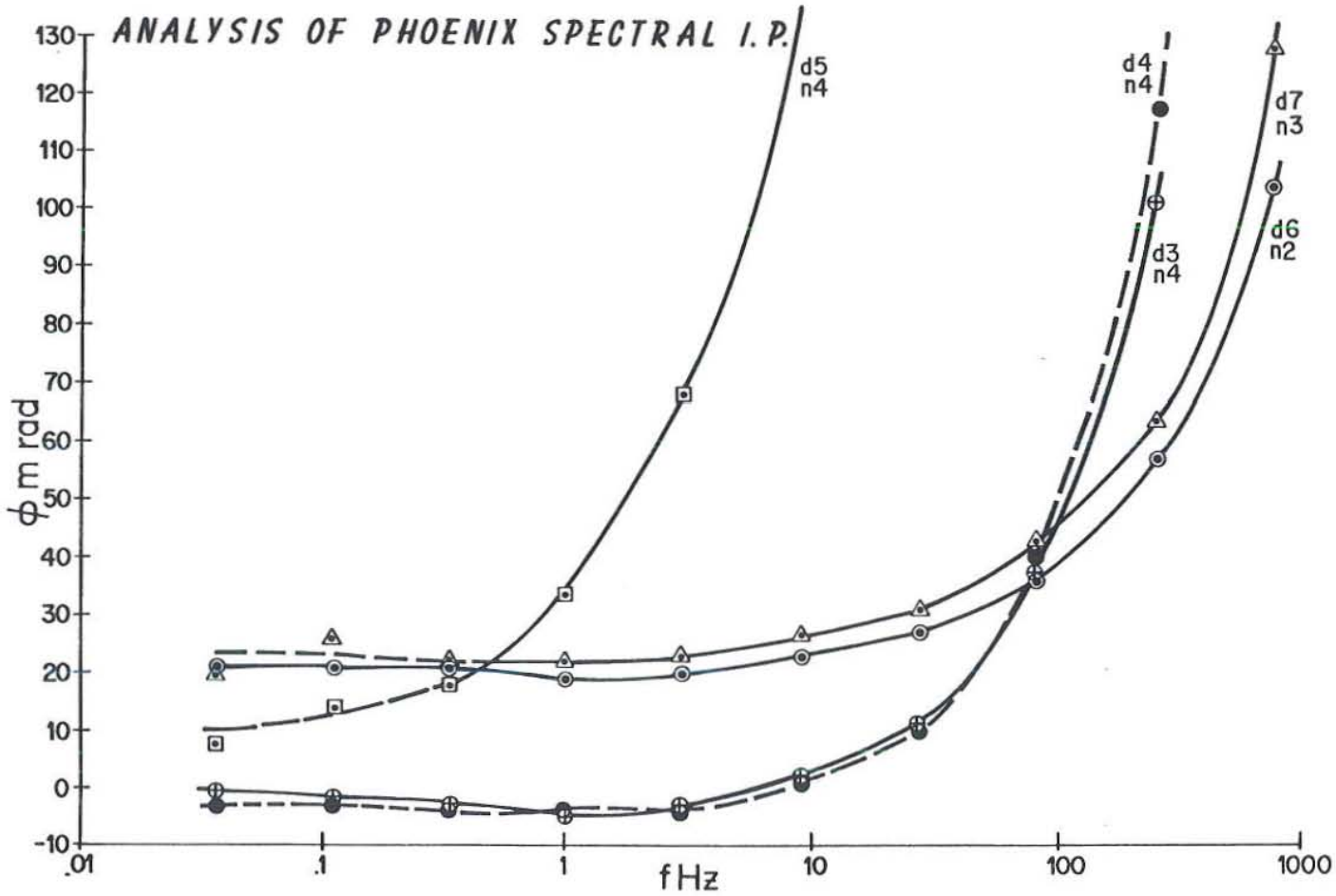

Fig. 15. Phase spectra for various dipoles and various spacings from IP survey in conductive terrane, Northern Territory, Australia. (Data by Phoenix Geophysics Ltd.).

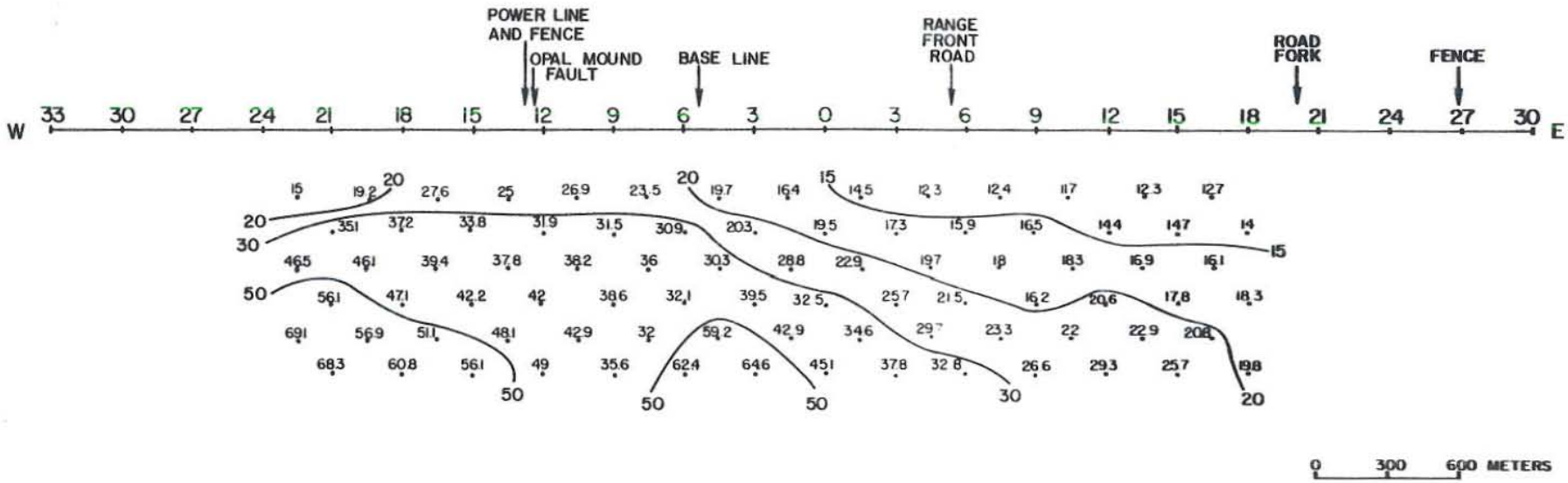

Line 1 (2200 N Road)
300 m dipoles
Phase pseudosection at 1/4 Hz
Contours at 1, 1.5, 2, 3, 5, 7, 10 ...
Location - Roosevelt Hot Springs

Fig. 16. Resistivity phase pseudosection at 1/4 Hz for Line 2200 N, Roosevelt Hot Springs, 300 m dipoles (after Chu et al., 1979).

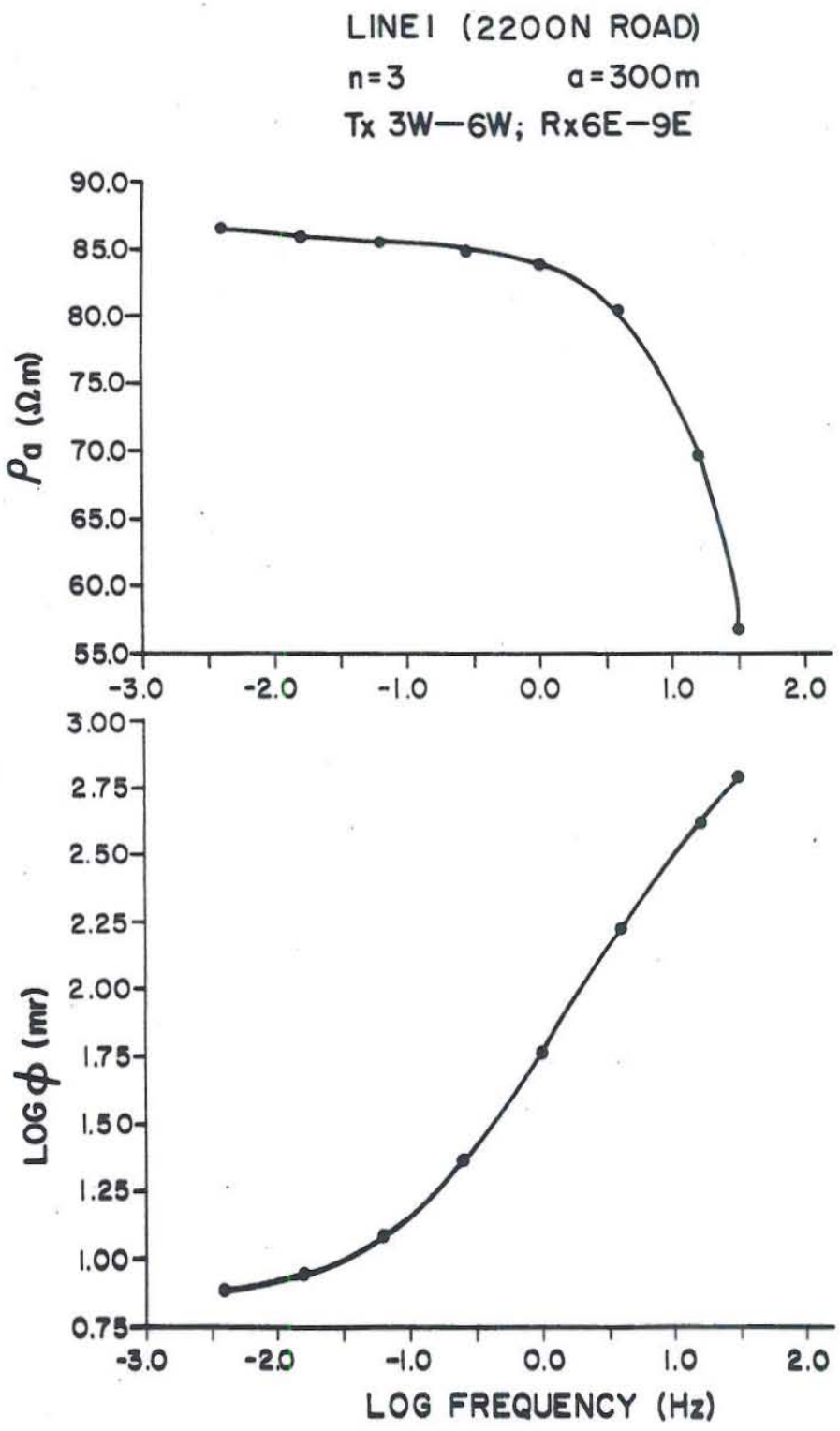

Fig. 17. Resistivity amplitude and phase versus log frequency for 300 m dipoles, Roosevelt Hot Springs (after Chu et al., 1979).

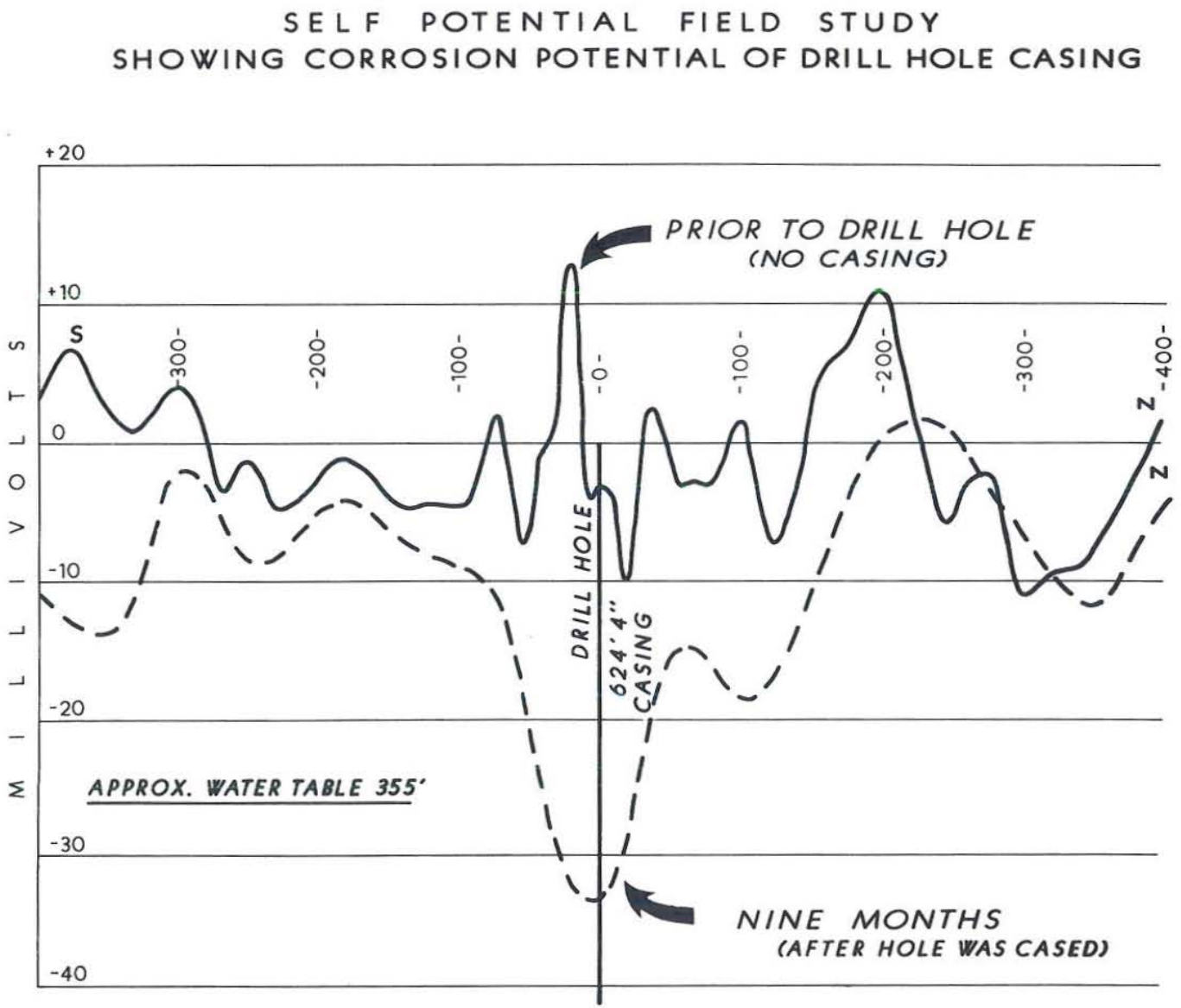

Fig. 18. Self-potential profile prior to and nine months subsequent to placement of casing in a drill hole (after Campbell, 1977).

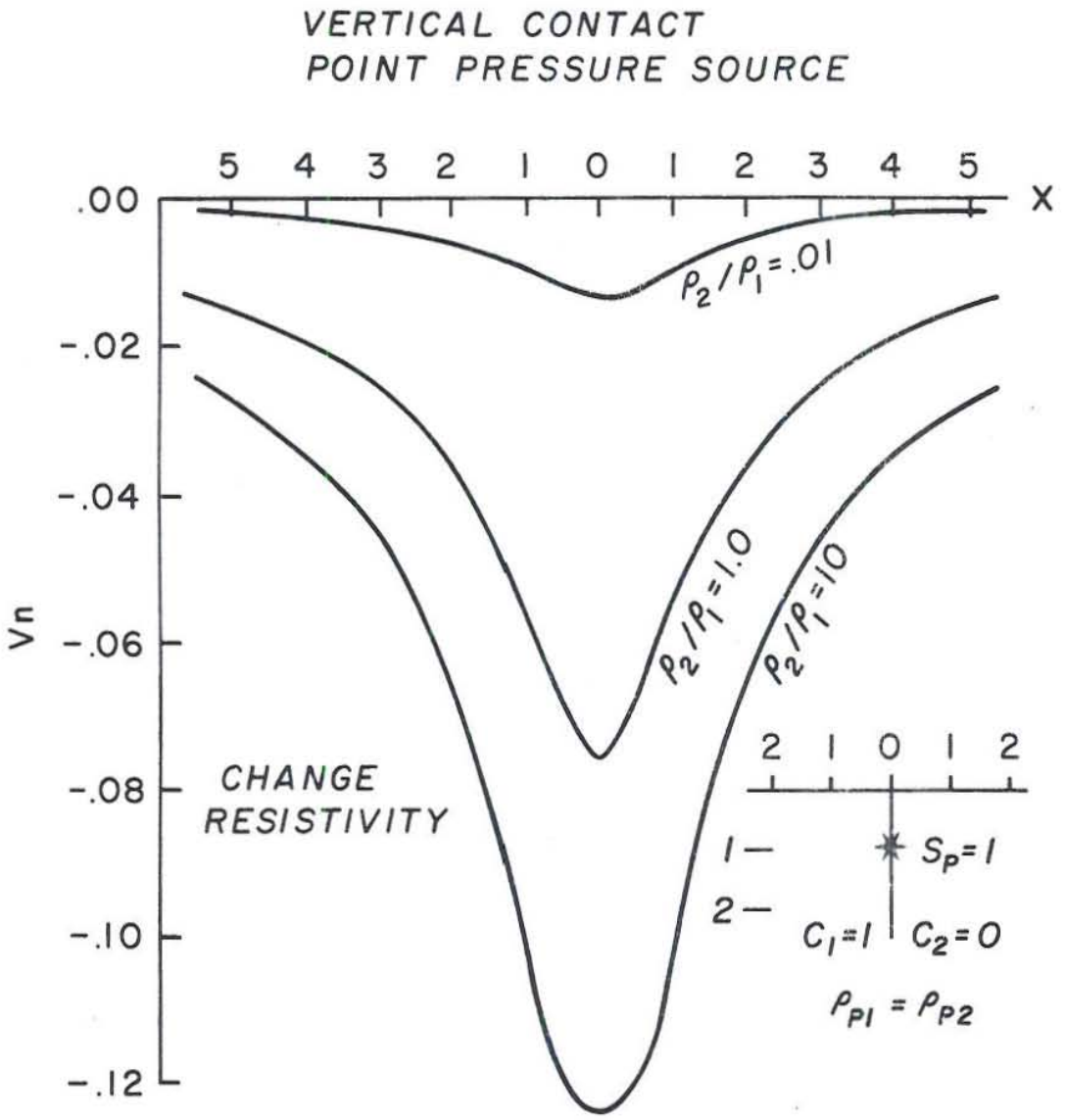

Fig. 19. Surface voltage for a point pressure source S_p located at a vertical contact. ρ_p is fluid resistivity, ρ^p is electrical resistivity, while C^p is the voltage coupling coefficient (after Sill, 1981).

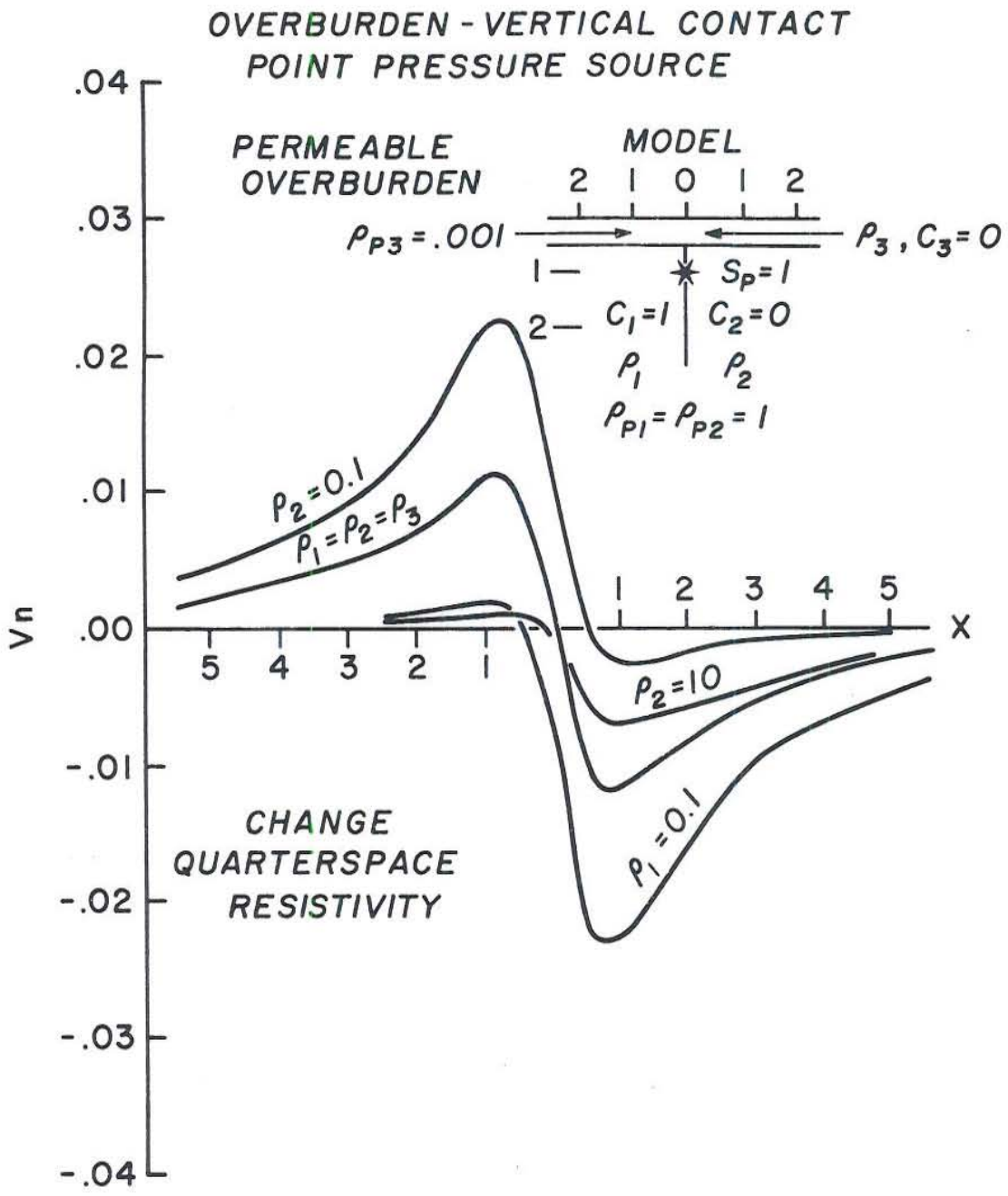

Fig. 20. Surface voltage for a point pressure source S_p located at a vertical contact covered by overburden. ρ_p is fluid resistivity, ρ is electrical resistivity, while C is the voltage coupling coefficient (after Sill, 1981).

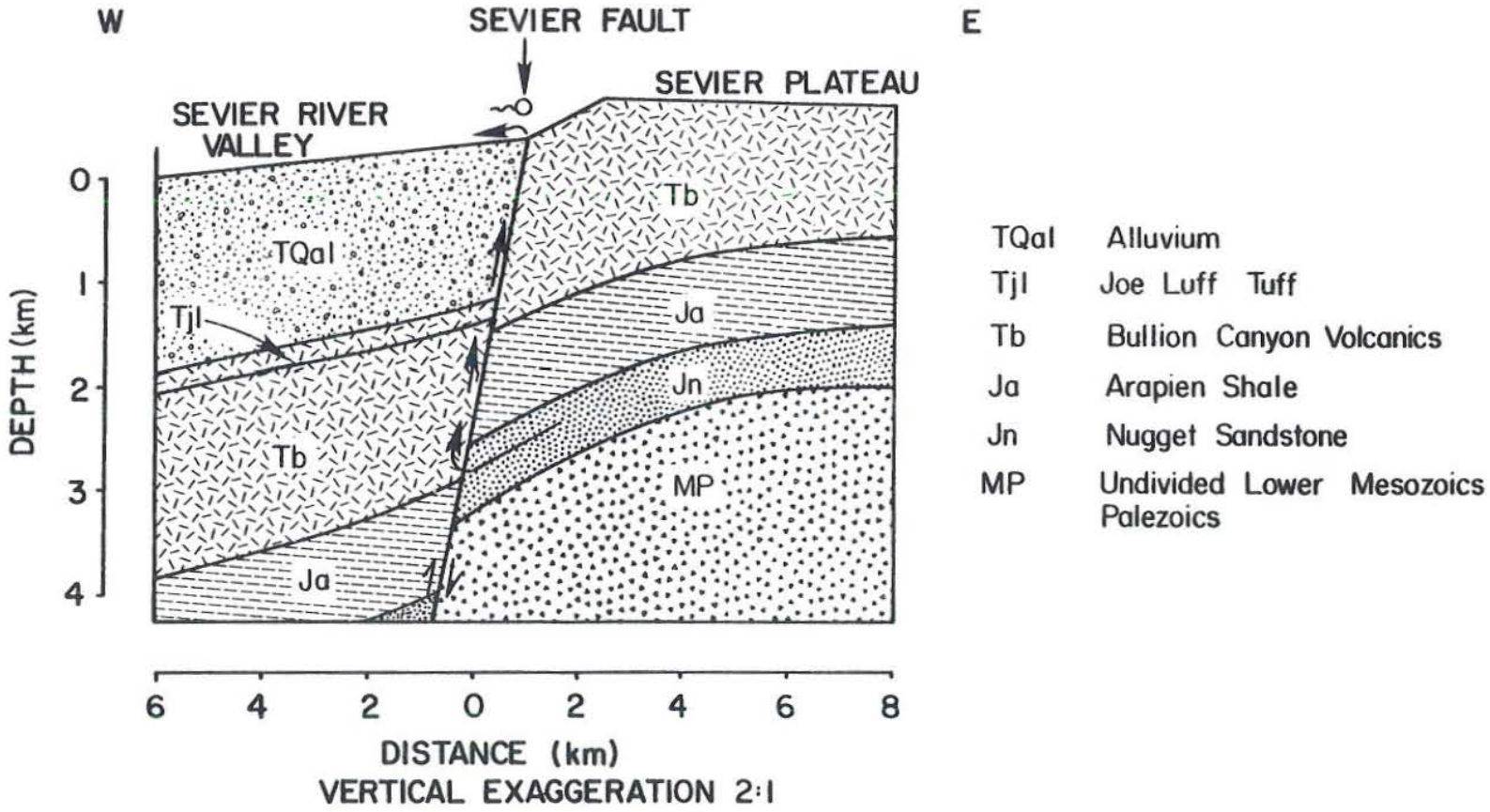

Fig. 21. Generalized geologic cross section of the Sevier Fault near Monroe, Utah, U. S. A. (after Mase et al., 1978).

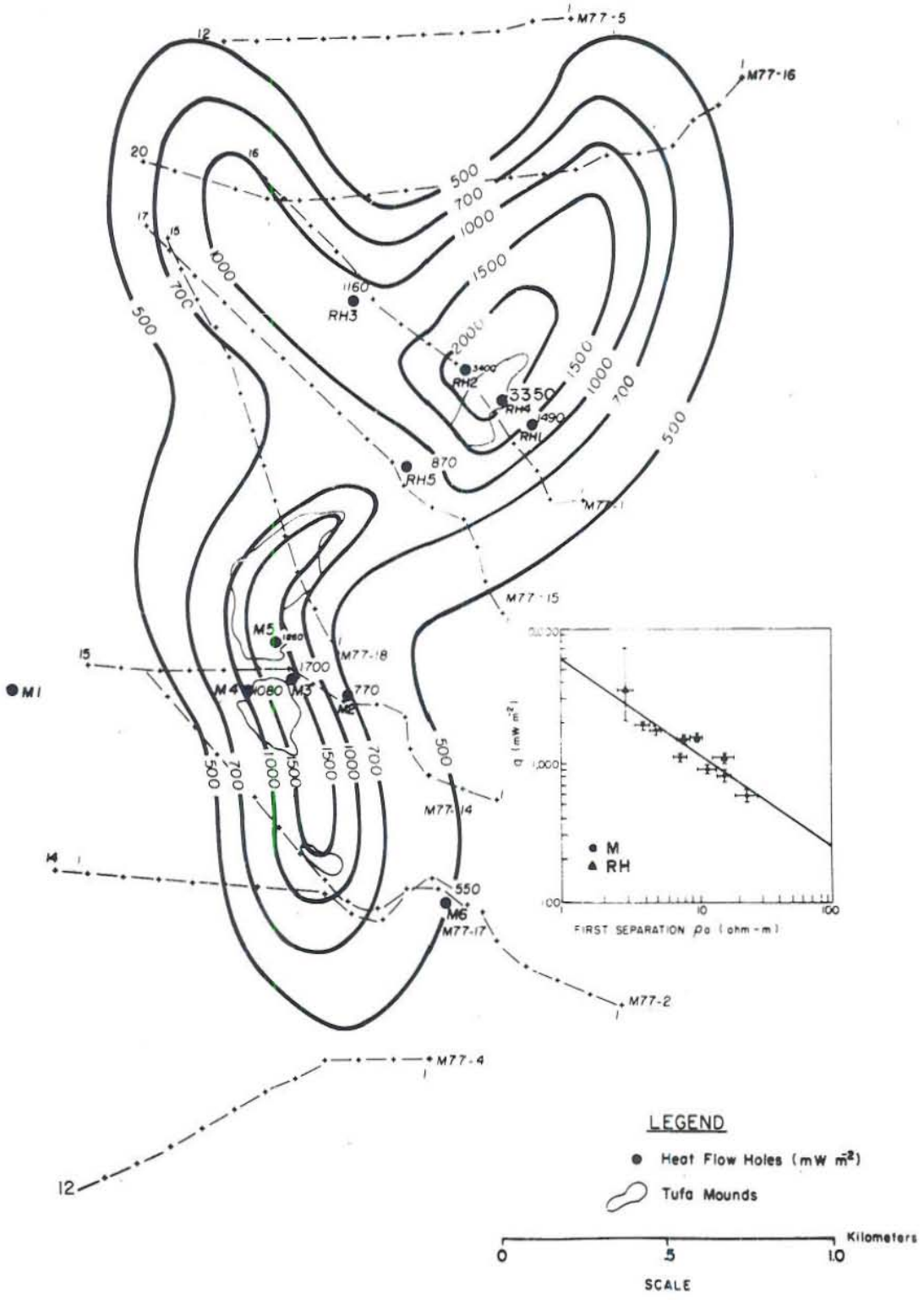

Fig. 22. Monroe-Red Hill heat flow map (after Mase et al., 1978).

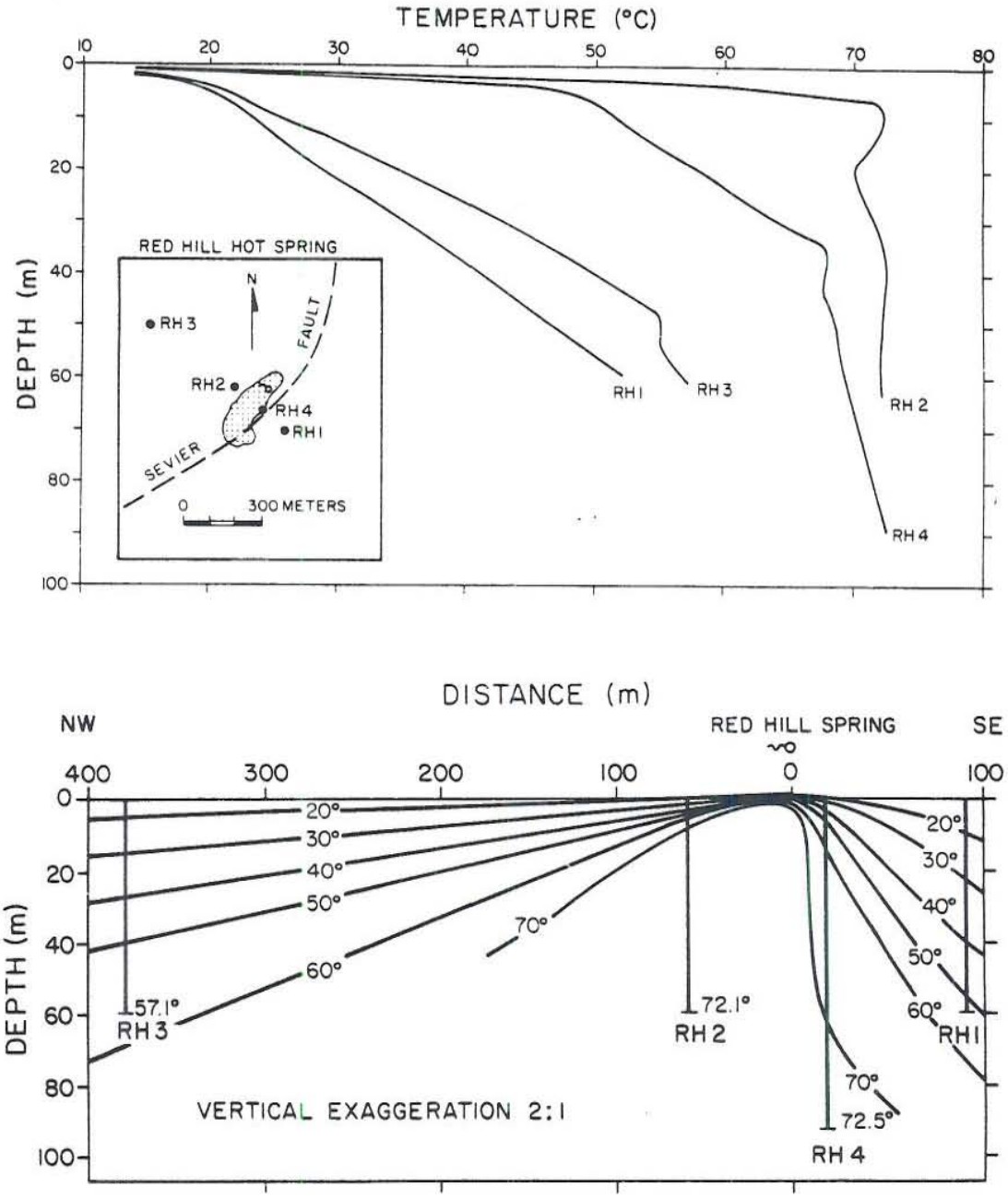

Fig. 23. Temperature-depth curves and isotherm cross section for Red Hill Hot Springs (after Mase et al., 1978).

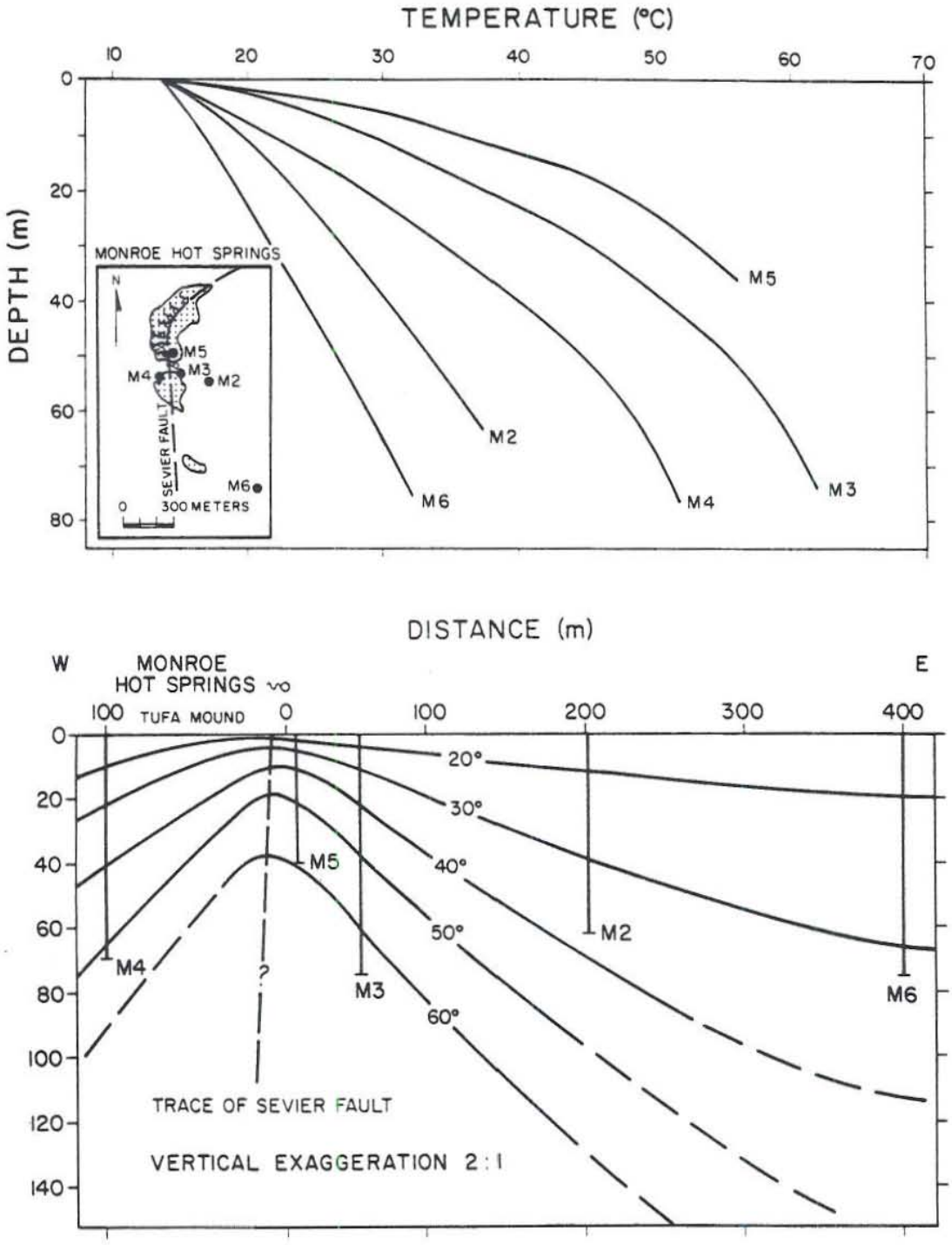

Fig. 24. Temperature-depth curves and isotherm cross section for Monroe Hot Springs (after Mase et al., 1978).

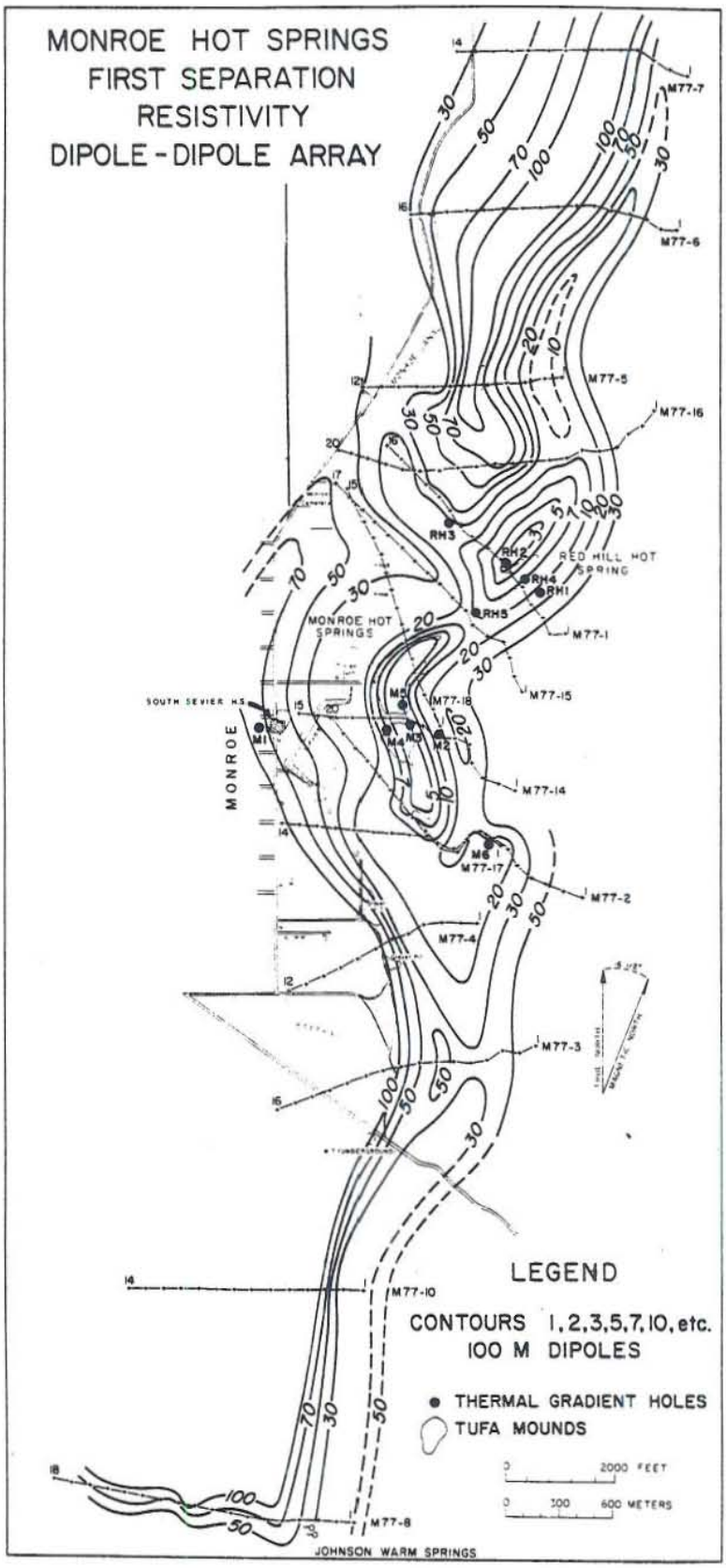

Fig. 25. Dipole-dipole first separation apparent resistivity contour map of the Monroe-Red Hill geothermal system (after Mase et al., 1978).

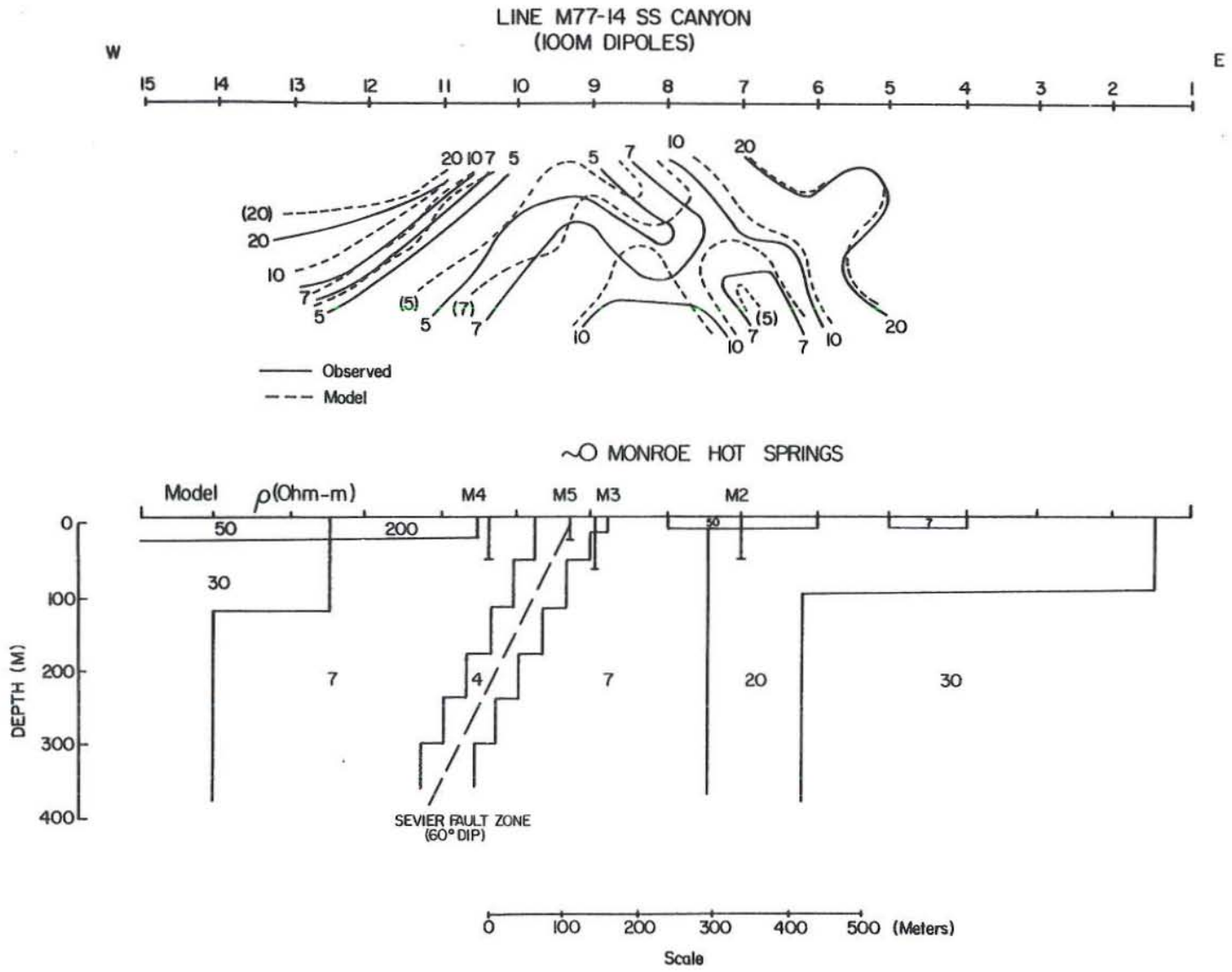

Fig. 26. Electrical resistivity model with 60° dip on the Sevier Fault, Monroe Hot Springs (after Mase et al., 1978).

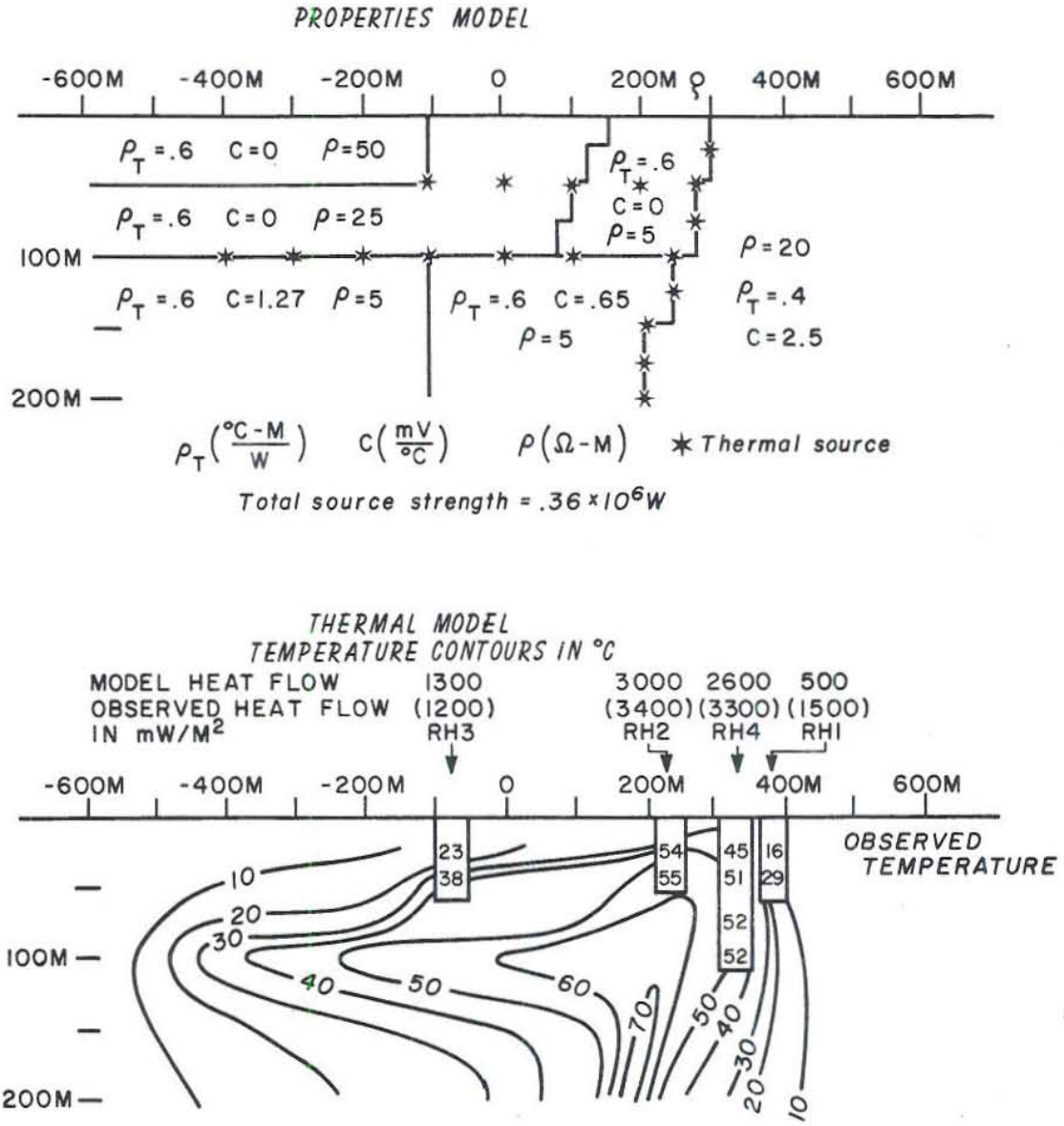

Fig. 27. (Top) Physical properties used to model the data at Red Hill Hot Springs ρ_T is thermal resistivity, ρ is electrical resistivity, C is voltage coupling coefficient.
(Bottom) Comparison of the observed and calculated temperatures at Red Hill Hot Springs (after Sill, 1981).

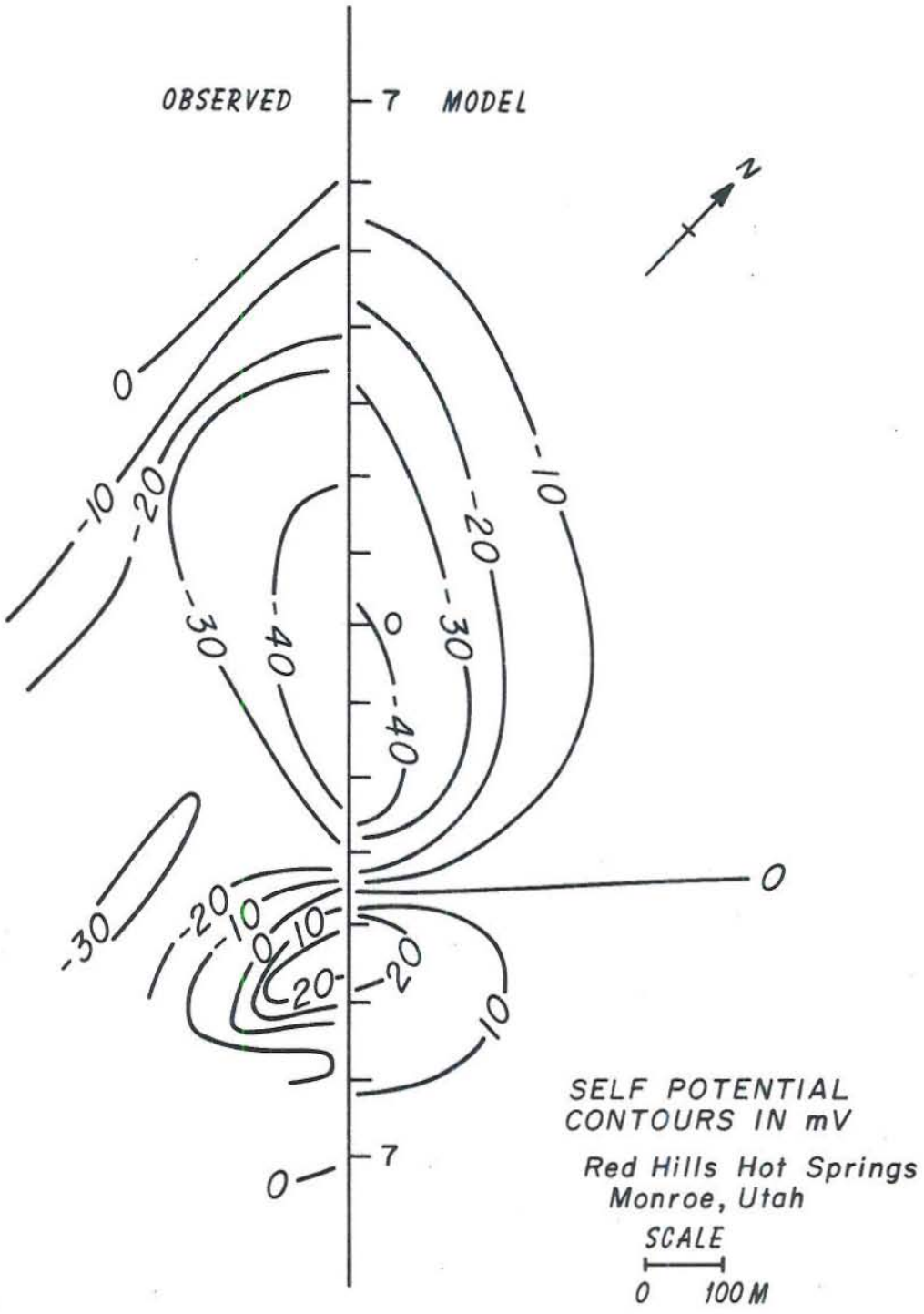

Fig. 28. Comparison of the observed and modeled self-potential anomaly at Red Hill Hot Springs.

14.0 LIST OF TABLES

TABLE 1

TYPE OF SEMICONDUCTION	σ_o	E	RANGE OF IMPORTANCE
EXTRINSIC	10^{-6} mho/m	1 ev	600°C
INTRINSIC	10^{-3} mho/m	3.3 ev	600 to 1,100°C
IONIC	10^{3} mho/m	3.0 ev	1,100°C

92

Table 1 Semiconduction follows the formula $\sigma=\sigma_0 e^{-E/kT}$ but σ_0 and E are different for each conduction mechanism. The values of σ_0 and E are stated here as are the temperature ranges of importance to each of the three mechanisms; extrinsic electronic, intrinsic electronic and ionic.

TABLE 2

BASIS FOR SELECTING P_a /IP ARRAYS

- TD OR FD
- DECADES OF SPECTRUM
- S/N RATIO
- LATERAL & VERTICAL RESOLUTION
- DEPTH OF EXPLORATION
- LATERAL EFFECTS
- EM COUPLING

93

Table 2 Factors to consider when selecting an array for resistivity and/or induced polarization surveys.

TABLE 3

RESISTIVITY ARRAY EVALUATION							
	SURF. EFF.	S/N RATIO	LAT. RES.	VERT. RES.	D. OF E.	LAT. EFF.	EM COUPLING
SCHLUMBERGER	1	1	3	1	3	3	3
POLE-DIPOLE	2	2	2	2	2	2	2
DIPOLE-DIPOLE	3	3	1	3	1	1	1

Table 3 A qualitative evaluation of major factors to consider when selecting an array for resistivity and/or induced polarization surveys.

TABLE 4

PROBLEMS WITH ρ_a / I.P.

- NATURAL FIELD NOISE
- CULTURAL NOISE
- EFFECT OF OVERBURDEN
- EFFECT OF OTHER GEOLOGIC NOISE
- EFFECT OF TOPOGRAPHY
- RESOLUTION, LATERAL AND VERTIICAL
- EM COUPLING
- NEED FOR MORE 2D, 2D-3D, AND 3D ALGORITHMS

Table 4 Problems with resistivity/induced polarization.

TABLE 5

CULTURAL NOISE

⇨ **PASSIVE**

- FENCES
- PIPELINES
- POWER LINES
- TELEPHONE LINES
- RAILS

⇨ **ACTIVE**

- POWER LINES
- TELEPHONE LINES
- ELECTRIFIED RAILS

Table 5 Sources of cultural noise.

TABLE 6

GEOTRONICS DR-I

FREQUENCY DOMAIN

- 0.001 Hz to 2000 Hz in 1,2,3.3,5 STEPS

SEQUENCE

- AUTOMATIC GAIN RANGING
- AUTOMATIC S.P. BUCKOUT
- SAMPLE at M PTS PER CYLE
  M=512, $f \leq 10$Hz
  DECREASING to 8 for f=2000Hz
- STACK N CYCLES
  AUTO—N=32 $f \leq 0.33$Hz
  N=64 $0.5 \leq f \leq 10$Hz
  INCREASE to N=1024
  $20 \leq f \leq 2000$

  MANUAL-ANY $N=2^n$ $n \leq 10$ ($f \leq 0.33$Hz)
- COMPUTE $|\rho a|$ and EXTRAPOLATE PHASE
- COMPUTE RUNNING STD. DEV. for $f \leq 0.33$Hz
- FULL PHASE and AMPLITUDE CALIBRATION

Table 6 Features of a microprocessor-based resistivity/induced polarization receiver.

TABLE 7

FEATURES OF MICROPROCESSOR BASED TRANSMITTER

- COMPUTER CONROL MONITORS ALL POWER CIRCUITS
- CONTROLS LOAD UP
- MONITORS INPUT POWER
- ABRUPT LOAD CHANGE SHUTDOWN
- DISPLAYS ALL OPERATING PARAMETERS
- ANALYZES SYSTEM FAULTS
- MAKES OPERATIONAL LOGS
- PROGRAMMABLE WAVEFORM
- FACILITATES REMOTE CONTROL

Table 7 Features of a microprocessor-based resistivity/induced polarization transmitter.

TABLE 8

NOISE IN SELF POTENTIAL SURVEYS

- TELLURIC
- ELECTRODE DRIFT
- TOPOGRAPHIC EFFECTS
- VARIATIONS IN SOIL MOISTURE
- CULTURAL NOISE
- VEGETATION POTENTIALS
- ELECTROKINETIC POTENTIALS, SURFACE WATER

Table 8 Noise in self-potential surveys.

TABLE 9

CULTURAL NOISE, S.P. SURVEYS

RADIATED FIELDS

- Power Lines
- Telephone Lines
- Electrified Rails

CORROSION POTENTIALS

- Pipelines
- Fences
- Well Casings

CORROSION PROTECTION SYSTEMS

- Pipelines

Table 9 Cultural noise in self-potential surveys.